

Article

An Investigation of Antimicrobial Activity for Plant Pathogens by Green-Synthesized Silver Nanoparticles Using *Azadirachta indica* and *Mangifera indica*

Archana Rana ^{1,2}, Anjali Kumari ^{3,4}, Amit Kumar Chaudhary ^{1,2}, Ritu Srivastava ^{1,2}, Deeba Kamil ^{3,4}, Parth Vashishtha ^{5,*} and Shailesh Narain Sharma ^{1,2,*}

¹ CSIR-National Physical Laboratory, Dr. K.S. Krishnan Marg, New Delhi 110012, India

² Academy of Scientific and Innovative Research (AcSIR), Ghaziabad 201002, India

³ SHUATS—Sam Higginbottom University of Agriculture, Technology, and Sciences, Allahabad 211007, Uttar Pradesh, India

⁴ IARI—Indian Agricultural Research Institute, Pusa, New Delhi 110012, India

⁵ Quantum Science Ltd., Keckwick Lane, Daresbury Office S03, Techspace One, Sci-Tech, Warrington WA4 4AB, UK

* Correspondence: parth@qscis.com (P.V.); shailesh@nplindia.org (S.N.S.)

Abstract: Photo-microbes are well known to demolish rice and fruits, as farmers use chemical pesticides to overcome agricultural problems and economic damage. The use of pesticides in agriculture fails to protect crops in lower concentrations and increases the intake of chemicals that cause many human ailments. The sophisticated nanotechnology approach used in agriculture for antimicrobial activities offers several advantages for growth and improves nutrient absorption in plants. We report the green synthesis of silver nanoparticles (AgNPs) using *Azadirachta indica* (*A. indica*) and *Mangifera indica* (*M. indica*) tree leaf extract that contains antioxidants to treat numerous diseases. AgNPs tested against three plant pathogens, fungi *Alternaria alternata* (*A. alternata*), *Sclerotium rolfsii* (*A. rolfsii*), and bacteria *Xanthomonas oryzae* (*X. oryzae*), which leads to agricultural problems. The experiment was performed with different concentrations of AgNPs in $\mu\text{L}/\text{mL}$ prepared using two other plants extract against fungi and bacteria during summer. The results expose the importance of plant extract in synthesizing silver nanoparticles (AgNPs) and their efficacy for microbes. A comparison among different concentrations of AgNPs (4 $\mu\text{L}/\text{mL}$, 6 $\mu\text{L}/\text{mL}$, and 10 $\mu\text{L}/\text{mL}$) was performed for two fungi (tomato disease) and bacteria (rice leaf blight disease). *A*-AgNPs (*A. indica*-AgNPs) demonstrate a greater zone of inhibition than *M*-AgNPs (*M. indica*-AgNPs), further highlighting the dependence of plants. Under in vitro conditions, the results of the antifungal activity showed zones of inhibition of 21 mm against *A. alternata* and 17 mm against *A. rolfsii*, while antibacterial activity against *X. oryzae* bacteria showed a 15 mm zone of inhibition at 10 mg/mL for *A*-AgNPs, and less for *M*-AgNPs. For AgNPs, the antifungal activity was characterized by a more significant area of inhibition than antibacterial activity was. The current study indicates that AgNPs with lower concentrations exhibit superior toxicity to microbes and may be able to manage diseases in rice and tomato, and increase plant growth.

Keywords: plant extract; *A. alternata*; *A. rolfsii* fungi; *X. oryzae* bacteria; silver nanoparticles



Citation: Rana, A.; Kumari, A.; Chaudhary, A.K.; Srivastava, R.; Kamil, D.; Vashishtha, P.; Sharma, S.N. An Investigation of Antimicrobial Activity for Plant Pathogens by Green-Synthesized Silver Nanoparticles Using *Azadirachta indica* and *Mangifera indica*. *Physchem* **2023**, *3*, 125–146. <https://doi.org/10.3390/physchem3010010>

Academic Editor: Klemen Bohinc

Received: 20 November 2022

Revised: 27 January 2023

Accepted: 3 February 2023

Published: 15 February 2023



Copyright: © 2023 by the authors. Licensee MDPI, Basel, Switzerland. This article is an open access article distributed under the terms and conditions of the Creative Commons Attribution (CC BY) license (<https://creativecommons.org/licenses/by/4.0/>).

1. Introduction

Due to their catalytic performance, affordability, and biocompatible environment, AgNPs are widely used in biomedical, food, physical, and chemical applications [1]. NPs can be synthesized using chemical, physical and biological methods. Their different shapes and sizes, controlled at the nanoscale level ($1 < 10$ nm), depend on time, concentration, and temperature [2]. Despite several methods being available, green synthesis remains a priority in the face of environmental issues, and the hazardous chemicals used in the

time-intensive production process [3]. Nanotechnology offers a diverse range of products used in medications, water purification, basins, clothing, food packaging, textiles, bio-imaging, catalysis, photonics, hospital, and antimicrobial [4]. Green synthesis involves bacteria, fungi, algae, templates, and plants in place of synthetic chemicals, which provides more benefits to society and can also be synthesized easily at low temperatures without agglomeration and toxicity [5]. Different plants/trees contain phytochemicals that can vary between them, producing numerous benefits in real life. Hence, plant extracts used for synthesis are presented as being safe and budget-friendly when applied to microbial activity for plants. Plant extract-mediated NPs possess extraordinary properties, without causing side effects. Nanoparticles have been studied with respect to their importance for plant growth, antimicrobial activity, seed germination, and enhancement of crop collection [6]. Although fertilizers are crucial for crop growth, they also result in a decrease in fertility. An imbalance in the soil's minerals results in numerous human cycle mutations [7]. As a result, over 45% of crops are destroyed annually due to microbes and plants interacting to produce plant destruction [8].

Alternaria alternata (*A. alternata*), *Sclerotium rolfsii*, also known as *Athelia rolfsii* (*A. rolfsii*), and *Xanthomonas oryzae* (*X. oryzae*), are significant fungi and bacteria leading to contamination. The increase in the incidence of blights and leaf spots [9], severe asthma [10], bronchopulmonary mycosis [11], and respiratory infections caused by *A. alternata*, stem rot, groundnut, wheat, vegetables [12], and many more originating from *A. Rolfsii* fungi, which are unstoppable (the host being a GBP500 plant). These plant bacteria pose a severe threat to vegetables and crops by interacting with plant tissue, roots, water, cuts, and wounds resulting from damage by insects. *X. oryzae* (a bacterial leaf blight occurring on rice) decreases rice quality and causes crop losses of up to 81% [13]. Many Indians have used the benefits of plants to treat skin problems, toothaches, diabetes, cancer, heart disease, and many more ailments [14]. The strong band of SPR (surface plasmon resonance) observed in AgNPs based on the shape and size of the NPs demonstrates better antimicrobial activity. Plants are an essential source of nutrients, and their antimicrobial activity is improved with the use of AgNPs. These tree leaf extracts produce NPs during synthesis and added the benefits of NPs with their properties. An antibacterial effect on plant pathogens described as AgNPs' ability to inhibit pathogen development without endangering adjacent plant tissues. Plant-synthesized AgNPs have excellent production, long-term stability, and lower toxicity. The use of pesticides and fertilizers in agriculture poses a risk to human health in this environment. The introduction of NPs in agriculture has been reported by researchers as a result of their application against plant diseases [15]. Various studies have reported that the activity of AgNPs against plant pathogens is dependent on physical attributes such as size, shape, and phytochemicals. The antimicrobial activity of plant fungi and bacteria is informed by the different structures of the cells. Singh et al., studied the antimicrobial activity of AgNPs tested against plant pathogens (*Fusarium oxysporum*, *Collectotrichum gloeosporioides*, *Bacillus* sp., and *Enterobacter cloacae*). The highest antimicrobial activity was found for *E. cloacae* (8.6 mm) and *Bacillus* sp. (7.0 mm) fungi, with increases in the zone of inhibition reported with 20% and 30% plant extract (7.7 mm and 11.3 mm) for both fungi [16]. Aritonang et al., synthesized AgNPs (24 nm) using *Impatiens balsamina* and *Lantana camara* plants to exert antimicrobial activities [17]. Henriquez et al., synthesized AuNPs and AgNPs from plant extract with the aim of imparting agricultural protection against microbes that cause food and water-produced diseases [18]. Mohammed et al., synthesized AgNPs against *S. aureus*, *P. aeruginosa*, and *E. coli* bacteria with an average size of 67.8 nm, and with anticancer activities of 10–30 nm [19].

This paper describes the *in vitro* antimicrobial activity of AgNPs synthesized using *Azadirachta indica* (*A. indica*) and *Mangifera indica* (*M. indica*) leaf extracts. These trees of Indian origin are used to treat diseases without causing any adverse effects. An *in vitro* process confirmed the antimicrobial activity of AgNPs (green-synthesized) against three plant pathogenic fungi and bacteria. The morphology, size, and structure of the AgNPs were evaluated using scanning electron microscopy (SEM) and transmission electron microscopy

(TEM). The stability and optical analysis were examined using Zeta-potential and UV-Vis spectroscopy. The green-synthesized AgNPs showed potent antimicrobial activity against plant pathogens.

2. Methods

2.1. Chemicals and Plants

Silver Nitrate (AgNO_3) in the >99.9% assay percent range was purchased from Fisher Scientific USA. DPPH (2,2-diphenyl-1-picrylhydrazyl), *Streptomycin*, Dextrose, and Agar were purchased from Sigma-Aldrich (St. Louis, MO, USA). The fungus was grown in the lab, and bacteria were collected directly from the Indian Agricultural Research Institute (IARI) lab (New Delhi, India). *A. indica* and *M. indica* were predominantly grown swiftly in tropical climates on the National Physical Laboratory site. Both plants are native to several African nations and the Indian subcontinent. The classification of *A. indica* and *M. indica* is provided in the following table:

<i>Azadirachta indica</i>	<i>Mangifera indica</i>
Family: Meliaceae	Family: Anacardiaceae
Common name: Neem	Common name: Mango
Species: <i>A. indica</i>	Species: <i>M. indica</i>
Genus: <i>Azadirachta</i>	Genus: <i>Mangifera</i>

2.2. Pathogens

The antimicrobial activity of silver nanoparticles against two different fungus species (*A. alternata*) (*A. rolfsii*) and one bacterium (*X. oryzae*), provided by the IARI (Pusa Road, New Delhi, India), was studied. These pathogens spread a variety of diseases infectious to crops, vegetable plant, and humans.

2.3. Preparation of Plant Extract

Fresh tree leaves from two different plants were collected from the campus of the National Physical laboratory and washed twice thoroughly with distilled water, and then cleaned with tissue paper to remove dirt. The *A. indica* and *M. indica* leaves (15 g) were ground using a pestle and mortar and then mixed in deionized water (80 mL) before being boiled on a hot plate for 30 min at 70 °C in a beaker to obtain the extract. The extracts were further filtered with Whatman filter paper and stored in the freezer for further use.

2.4. Synthesis of Silver Nanoparticles

A total of 1 mM (millimolar) solution of AgNO_3 salt was dissolved in distilled water and added to leaf extract for reaction. The extract ratio would vary during the responses due to high phytochemicals. A total of 6 mL of extract from *A. indica* and *M. indica* leaves was added to 20 mL of 1 mM AgNO_3 solution to reduce the metal salt into metal nanoparticles. The reaction mixture was then heated at 60–70 °C for 15–20 min in a beaker, round bottom flask, or conical flask. The color of the NPs started changing from transparent to dark brown due to the formation of NPs, as shown in Figure 1. The synthesized AgNPs can be stored under 4 °C for one year to perform different characterizations [20].

2.5. Preparation of PDA Media

Potato dextrose media (PDA) were prepared using 20 gm Agar, 20 gm dextrose, potato extract (200 mL), and deionized water (800 mL). PDA media were separated in a different flask and then autoclaved for 3 h at 115 °C when the temperature (room temperature) of the PDA reached 35–40 °C for further use, and allowed to settle down (15 min) slowly in a petri dish.



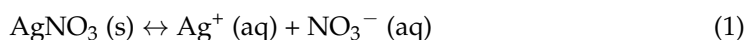
Figure 1. Synthesis of silver nanoparticles using different plants (*A. indica* and *M. indica*).

2.6. Isolation of Fungus and Bacteria

The samples of *A. alternata* and *A. rolfsii* fungus collected from the test tubes were isolated from fruits and plants. A small fungus sample and a pinch of *Streptomycin* were added to autoclaved PDA media at 35–40 °C. The fungus-mediated PDA media were poured into a petri dish to rest in solidifying. The growth of *A. alternata* and *A. rolfsii* (fresh fungus) on PDA (potato dextrose agar) was observed after seven days of inoculation at a temperature of ±27 °C. *X. oryzae* bacteria were isolated from the infected rice leaves, which exhibited symptoms of bacterial leaf blight illnesses, in order to study the in vitro susceptibility to the AgNPs. The isolated bacterial suspension was obtained from the cultures grown in nutrient broth overnight and further carried out to study against AgNPs.

2.7. Mechanism of Silver Nanoparticles

The natural phytochemicals in plants reduce metal salt to metal nanoparticles by oxidation and reduction methods in water. The addition of silver nitrate(s) to deionized water was mixed well in an aqueous form; Equation (1):



The aqueous silver nitrate was added to the plant extract to reduce silver cation (Ag^+) to silver nanoparticles. The transfer of electrons from phytochemicals to silver cations is shared in the form of radicals to each cation converting into nanoparticles (zero valences) and oxidizing itself. In Figure 2, gallic acid is used as an example, and is converted into 3, 4-didehydroshikimate, i.e., quinone, with the sequential process of the conversion of Ag^+ to Ag^0 NPs [21].

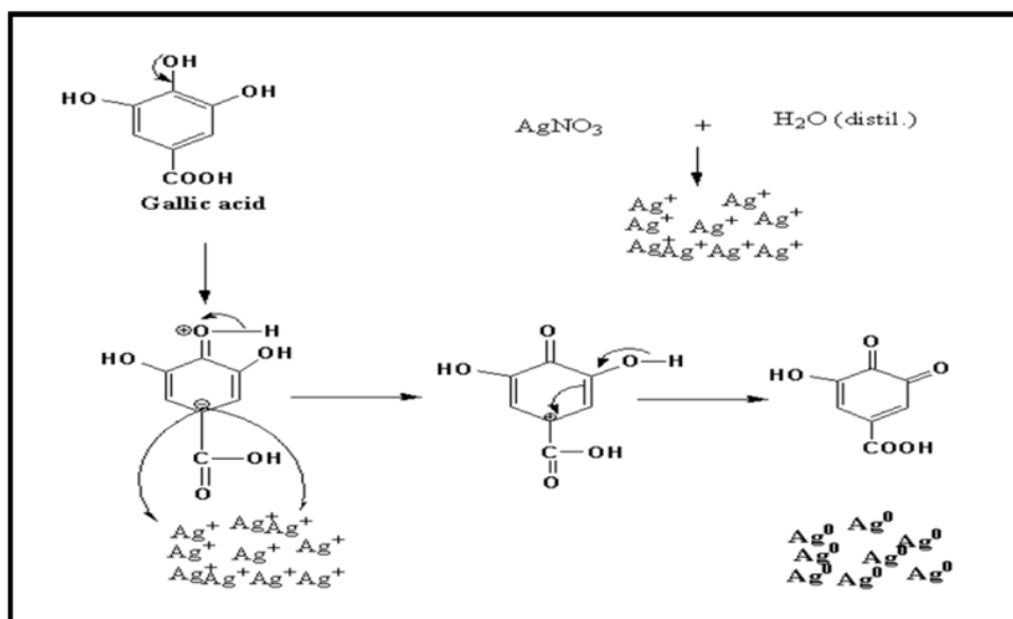


Figure 2. Mechanism for the reduction of AgNPs in presence of natural phytochemicals.

The current mechanism in Figure 2 was explained using gallic acid with Ag^+ cation. The functional groups in plant extract, such as hydroxyls, enone in catechins, and flavonoids, have been well-defined in the literature. The major reducing agents in (*Az. indica* and *Mg. indica*) plant extracts are flavonoids, catechins, saponins, azadirachtins, phenols, gallic acid, and alkaloids, as also shown in Table 1 [22,23].

Table 1. Phytochemical presence in aqueous extract of *A. indica* and *M. indica* leaves.

Natural Chemical	Presence	Natural Chemical	Presence
Azadirachtin	+	Gallic acid	+
Nimbins	+	Saponins	+
Flavonoids	+	Limonoids	+
Alkaloids	+	Nimboesterol	+
Phenols	+	Tannins	+
Steroids	+	Polyphenols	+

These antioxidants react with Ag^+ (cation) in the colloidal form and are reduced to Ag^0 NPs the moment plant extracts are added to the solution of silver nitrate at a certain temperature and concentration. This reaction is possible because of the presence of functional groups in the antioxidants that donate their electron to Ag^+ , oxidizing itself. After reduction, the atomic nuclei tend to assemble closely, initiating the process of NPs formation. The capping agent bound to the surface of the NPs when the NPs attain their maximum size stabilizes the surface energy [24]. Omidi et al. synthesized AgNPs using *adiantum capillus-veneris* L leaf extract and observed the presence of the phenolic group. The study demonstrated the reaction mechanism of flavonoids and polyphenols with Ag^+ to produce AgNPs by reacting with hydroxyl and converting them to a carbonyl group [25]. Similarly, Sharma et al. synthesized AgNPs using saponin seed extract (*Madhuca longifolia* seed extract) as a major constituent in the proposed mechanism to produce Ag^+ to AgNPs [26].

2.8. Antioxidant Assay

2.8.1. Free Radical 2, 2-diphenyl-1-picrylhydrazyl (DPPH) Scavenger

The presence of free radicals in DPPH produces a reaction with a hydrogen atom or electron provided by extract or silver nanoparticles modified by the fading of purple to a pale yellow color, as confirmed by UV-Vis spectrophotometer. A 0.2 mM volume of DPPH solution was mixed with *A. indica*, *M. indica* (plant extract), *A-AgNPs*, and *M-AgNPs* prepared at various concentrations: 50, 100, 150, 200, 250, 300, 350, 400, 450, and 500 mg/mL. Methanol was added to DPPH as a control. The mixture was vigorously swirled and incubated for 20 min at room temperature in the dark. A UV-Vis spectrophotometer was used to determine the solution's absorbance at 517 nm (Lambda 950). As it contained several antioxidants, ascorbic acid was employed as a standard. The following equation was utilized to estimate the free radical scavenging activity [27];

$$\% \text{ of DPPH Scavenging} = \frac{S_c - S_a}{S_c} \times 100 \quad (2)$$

where, S_c = absorbance of DPPH radical control, S_a = absorbance of DPPH radical with silver nanoparticles/ascorbic acid.

2.8.2. Phytochemical Presence in Different Plants

The several phytochemicals identified in the aqueous leaf extract of *A. indica* and *M. indica* tree leaves that cap and reduce silver salt to AgNPs have been the subject of substantial qualitative research. The studies show that phytochemical screening of *A. indica* and *M. indica* leaf extract suggest that they are a good source of activity against many

diseases, including oral cancer [28], as well as providing anti-fungal, anti-bacterial, and anti-diabetes effects, and working against ulcers, as can be observed in Figure 3 [29] studied the *A. indica* leaf powder to remove 98% malachite green dye from the industrial waste. Aqueous *A. indica* and *M. indica* extracts also prevent lung fibrosis and coagulopathy with regular usage. *A. indica* leaf extracts contain azadirachtin, phenols, hasnimbin, quercetin, limonoids, and tannins, and *M. indica* extracts contain mangiferin, catechin, gallic acid, flavonoids, and hyperin [22,23]. These antioxidants react with Ag^+ (cation) in colloidal form and are reduced to Ag^0 NPs, the moment plant extracts are added to the silver nitrate solution at a certain temperature and concentration. The reaction is possible because of the presence of functional groups in the antioxidants to donate their electrons to Ag^+ and oxidize themselves. After reduction, the atomic nuclei tend to assemble closely, initiating the process of NPs formation. The capping agent bound to the surface of NPs when the NPs attained the maximum size, stabilizing the surface energy [24].

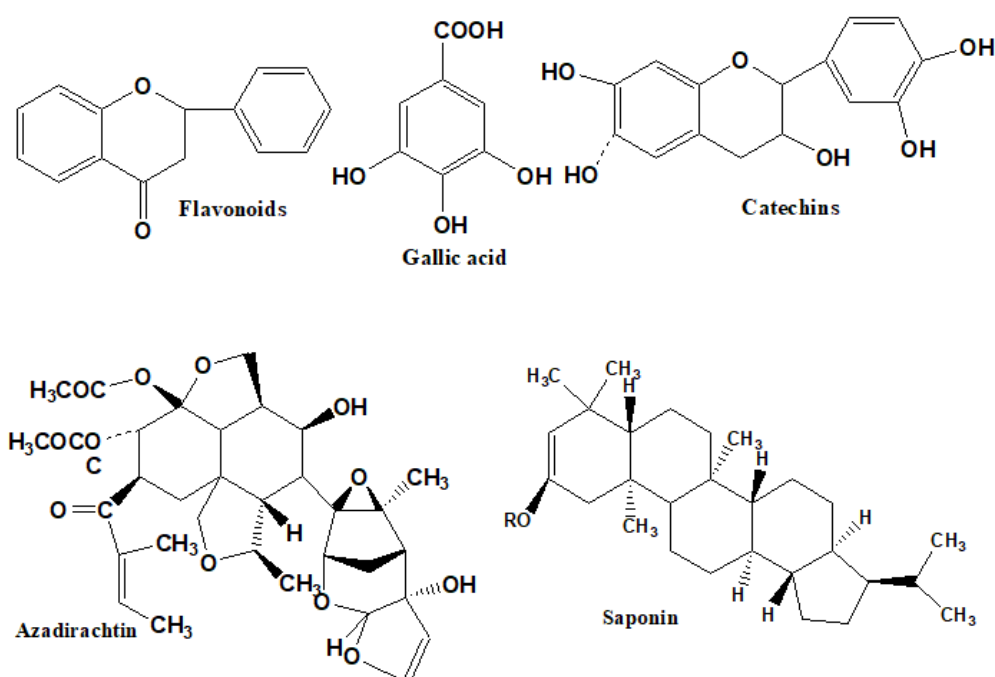


Figure 3. Portrait of the phytochemicals present in *A. indica* and *M. indica* tree leaves using ChemDraw Ultra 8.0 software.

3. Characterization of the Synthesized AgNPs

The reduction of silver Metal (M^+ to M^0 NPs) was confirmed by measuring the UV-Vis spectroscopy of the low ratio of nanoparticles following dilution in distilled water. The color changed from transparent to brown following the completion of the reactions. A UV-Vis instrument (Shimadzu UV-3101) was used to measure the absorbance between 300 nm and 800 nm [Duisburg, Germany].

GIXRD (Grazing Incidence X-ray diffraction) patterns were recorded using a high-precision PANalytical X'Pert PRO MRD [United Kingdom] high-resolution system with $\text{Cu K}\alpha$ with $\lambda = 1.54059 \text{ \AA}$ radiation scanned in 2θ ranges from 20 to 80° . The Scherrer equation was also used to analyze particle size (Equation (3)):

$$\iota = k\lambda / \beta \cos\theta \quad (3)$$

where, ι = average size of ordered domains, λ = wavelength of radiation, k = dimensionless shape factor (Scherrer constant), β = full width at half maximum in radians, and θ = angle diffraction.

The nanoparticles' size and morphology were measured using a TEM (transmission electron microscopy) instrument from Jeol Ltd. [Tokyo, Japan], with an accelerating voltage

of 100 kV. The nanoparticles used for TEM analysis were ultra-sonicated for 15 min, and then the AgNPs were dropped onto a carbon-coated copper grid to let them dry in air. SEM (scanning electron microscopy) measurements (ZEISS instrument) [Jena, Germany] of the nanoparticles were performed in order to study their morphologies. SEM (scanning electron microscopy) was employed to determine the surface morphology of the AgNPs.

FTIR (Fourier-transform infrared) spectral analysis (Perkin Elmer FTIR spectrum BX-II) was performed to identify the presence of functional groups, measured in the range 400–4000 cm^{-1} , with maximum output being less than 1 mW with 64 scans, recorded in transmission mode [Germany]. The organic phytochemicals present in silver nanoparticles prepared in KBr salt were added to a small number of nanoparticles in order to prepare the pellet. The hydrodynamic diameter and stability of the nanoparticles were measured using a DLS (dynamic light scattering) instrument (Malvern Panalytical) [Austria]. The particle size was obtained using a Malvern (1062761) Zetasizer at 25 °C with a measurement position of 2 mm in an aqueous medium [Austria].

4. Antimicrobial Activity

4.1. Anti-Fungal Activity

The standard disc diffusion method was performed with the antifungal assays against *A. alternata* and *A. rolfsii* fungicide. *A. alternata* and *A. rolfsii* fungicides were added in a separate conical flask and mixed thoroughly by agitating slowly. The mixture was poured (10 mL) directly on auto-clave petri dishes. The autoclaved filter paper disc of 4 mm diameter soaked in AgNPs (varying concentration) was placed on each plate for antifungal resistance. The plates were incubated at 27 °C for four days until the growth of fungicides, and zone of inhibitions around the discs were noted and scaled.

4.2. Anti-Bacterial Activity

Martinus Beijerinck and Perez introduced the anti-bacterial activity method by disc diffusion method discovered in 1889 [30]. The *A-AgNPs* and *M-AgNPs* were examined against the *X. Oryzae* strain with respect to their anti-bacterial activity. The sterilized PDA (200 mL) was poured into various autoclaved Petri plates. Fresh inoculum of bacterial (150 mL) strains was spread onto multiple petri plates (with numbering) using a sanitized spreader to cultivate bacterial growth. The autoclaved 4 mm filter paper discs were pierced on PDA media infused with different concentrations of *A-AgNPs* and *M-AgNPs* (3.0, 6.0, and 10 $\mu\text{L}/\text{mL}$), and deionized water was used as control. Bacterial growth was observed following incubation for 48 h at 37 °C. The zone of inhibition was measured around the well, and the studies were conducted twice against each bacterium to verify the solidity and record the measurements. The correlation of the mean inhibitions of plant pathogen growth were analyzed using ANOVA (one-way analysis of variance), with significant differences in activity being determined using a *t*-test ($p < 0.05$).

5. Results

The green synthesis of AgNPs produced using different plant leaf extracts (*A. indica* and *M. indica*) occurs due to reduction of silver salt (precursor) to NPs by biomolecules. The change in the color of the reaction mixture from transparent to brown during synthesis has been reported in many studies [31]. The intensity of synthesized AgNPs was scrutinized using different parameters.

5.1. Optical Analysis

Optical analysis was performed by means of UV-Visible spectroscopy characterization for the peak spectrum of AgNPs at a concentration of 1 mM AgNO_3 . The absorption of plant-mediated AgNPs was measured using a UV-Vis spectroscopy instrument ranging from 350 to 600 nm. The absorbance peak, observed at 432 nm (*A-AgNPs*) and 442 nm (*M-AgNPs*), as shown in (Figure 4a,b), indicates the formation of AgNPs and the presence of free electrons on the surface of the nanoparticles, known as surface plasmon resonance

(SPR), which is produced by the vibration of the nanoparticles. The spectrum confirms a single sharp peak for both plant-mediated AgNPs, without extra peaks, also confirming that the NPs are spherical in shape. The absorption spectra of the NPs were used to analyze the intra-band excitations of conduction electrons in the AgNPs, from lowest to highest energy state [32]. The formation of AgNPs occurs due to the enhancement of SPR band intensity, which shifts from red to blue, resulting in an increase in the size of the NPs. According to previous research, the surface plasmon resonance of AgNPs causes an absorption peak in the range between 420 and 450 nm [33]. Similar studies have been reported for AgNPs synthesized using *Ocimum sanctum* extract, for which SPR absorption takes place at 445 nm, with a sharp peak indicating the small size of the NPs [34]. The uniform shape of the SPR band demonstrates the spherical shape of the AgNPs. The surfaces of the AgNPs resemble plasmon due to their positively charged nuclei and unbound electrons in the conduction band [35]. Mangini et al., studied the interaction of ubiquity with AgNPs using the laser ablation method, showing the shifting of the SPR band to a higher wavelength, such that more extensive aggregation and distribution changes in the NPs could be observed [36]. Khannanov et al., first reported the magnetic properties of Cobalt nanoparticles using the hyper-branched polyester polyol to enhance the proteolytic enzymes. It was observed in their study that the SPR range indicates the formation of Cobalt nanoparticles in the range of 257–276 nm [37]. The higher concentration of phytochemicals (organic molecules present in extract), colloidal uniformity, particle size, and presence of delicate AgNPs are the factors responsible for the broad absorption peak [38]. The color change in the AgNO₃ salt and leaf extract from transparent to brown is dependent on temperature, concentration, and reaction time. The addition of plant extract at higher concentration decreases the chances of AgNPs formation. The growth of AgNPs from the reduction of metal salt follows the pattern of Ostwald ripening. The plasmon peak depends on the dielectric constant:

$$\lambda_{sp}^2 = \lambda_p^2(\epsilon_\infty + 2\epsilon_m) \quad (4)$$

where ϵ_∞ = high-frequency dielectric constant; ϵ_m = surrounding medium; λ_{sp} = plasmon peak position; and λ_p = bulk plasmon frequency [39].

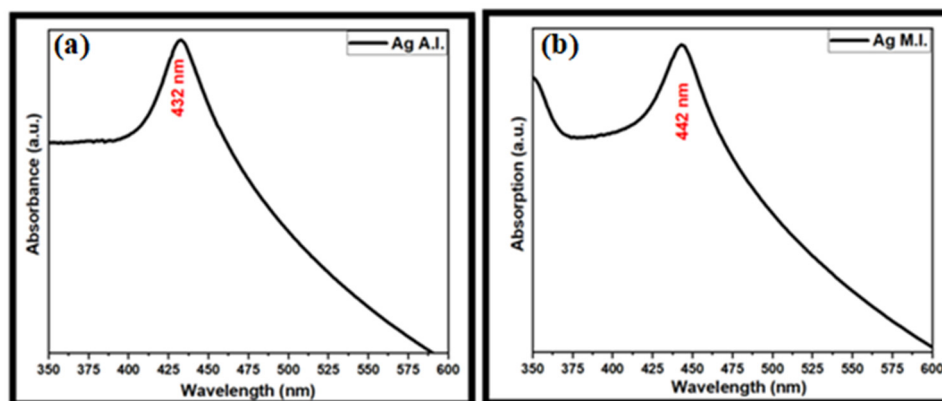


Figure 4. UV-Vis absorbance spectrum of AgNPs as a function of 1 mM AgNO₃ concentration in aqueous extracts of fresh leaves of *A. indica* (a) and *M. indica* (b) tree.

5.2. GIXRD (Grazing Incidence X-ray Diffraction)

GIXRD was used to perform the structural analysis of green-synthesized AgNPs using *A. indica* and *M. indica* tree leaves. Four diffraction peaks were observed at $2\theta = 38.12, 44.27, 64.54,$ and 77.29 , as shown in (Figure 5a,b) at a scan range of $20 < 2\theta < 80^\circ$. The major peaks in the spectra correspond to the (111), (200), (220), and (311) planes, possessing an fcc (face-centered cubic) structure, and resembling JCPDS card no: 04-0783 [40]. The spectra of the AgNPs (*A. Indica* and *M. Indica*) were compared using the JCPDS Ag/Ag₂O NPs range. No additional impurity peaks (oxides) were observed in the spectra, indicating the presence of AgNPs only [41]. Manikandan et al. synthesized Ag₂O NPs and studied

them against dental pathogens, showing the XRD spectrum peaks for both Ag/Ag₂O NPs [42]. Archana et al. synthesized Ag₂O NPs using *Artocarpus Hetrophyllus* plant extract and analyzed their antibacterial activity, showing diffraction planes for silver and oxide NPs [43].

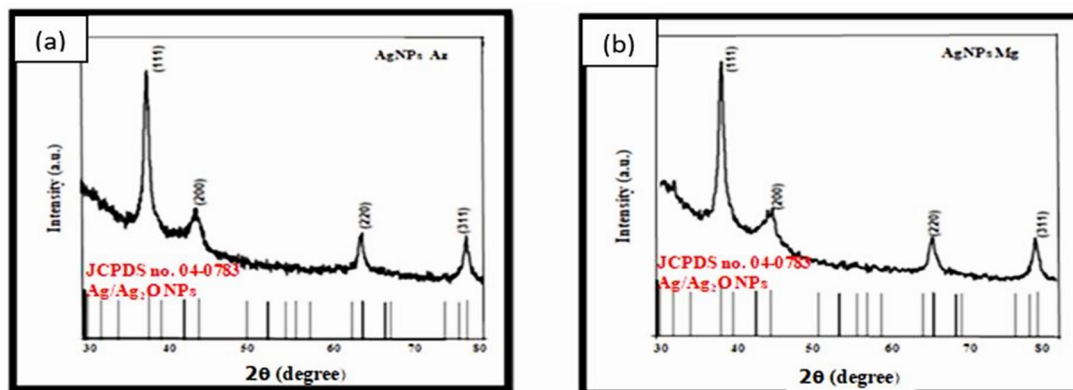


Figure 5. XRD pattern of the (a) *A-AgNPs* and (b) *M-AgNPs* synthesized from tree leaf extract.

The crystallite size of the colloidal AgNPs was evaluated using Debye Scherrer's formula:

$$d = \frac{0.94\lambda}{\beta \cos \theta} \quad (5)$$

where β denotes the broadening of diffraction lines, λ is the wavelength (0.1546 nm), and θ represents Bragg's diffraction angle.

The sharp peaks indicate the spherical shape and crystalline nature of the nanoparticles. As calculated by Debye Scherrer's formula, the average crystallite size for *A-AgNPs* and *M-AgNPs* are 9.4 nm and 9.8 nm. The small crystallite size increases the interior volume and surface area, causing nanoparticles lattice contraction [44]. The crystallite size coincides with the orderly coherent diffraction domain, which is always smaller than the TEM. The highest peak, which is at 38.12 in both spectra, describes the actual growth and purity of the AgNPs [45].

The sharpening of the peaks exhibits a size in the nano regime, and indicates the crystalline nature of the NPs [46].

5.3. TEM (Size and Shape)

TEM characterization was used to investigate the shape of *A-AgNPs* and *M-AgNPs*, and their precise size information. The colloidal solution of *A-AgNPs* and *M-AgNPs* was deposited on a carbon-coated grid and dried under normal conditions. The green-synthesized AgNPs were quasi-spherical (high surface area), grown thermodynamically, and anisotropic. The capping agents in phytochemicals enhance monodispersity and crystal growth [46]. The recorded images demonstrated the presence of mono-dispersed nanoparticles with a spherical shape. The size and shape of the nanoparticles are important factors in their antimicrobial activity; smaller particles can easily interact with the cell walls of micro-organisms (RNA and DNA) [47]. The green-synthesized AgNPs were spherical, with average particle sizes of 11.45 nm (*A-AgNPs*), as shown in Figure 6a–c, including a histogram of size distribution, and 22 nm (*M-AgNPs*), as shown in Figure 6d–f. The size calculated on the basis of TEM is always smaller than that calculated using DLS. The DLS was used to calculate the hydrodynamic diameter of AgNPs with their capping agents and reducing agents in the form of the phytochemicals present in the vicinity of NPs, whereas TEM directly provides size and structural information.

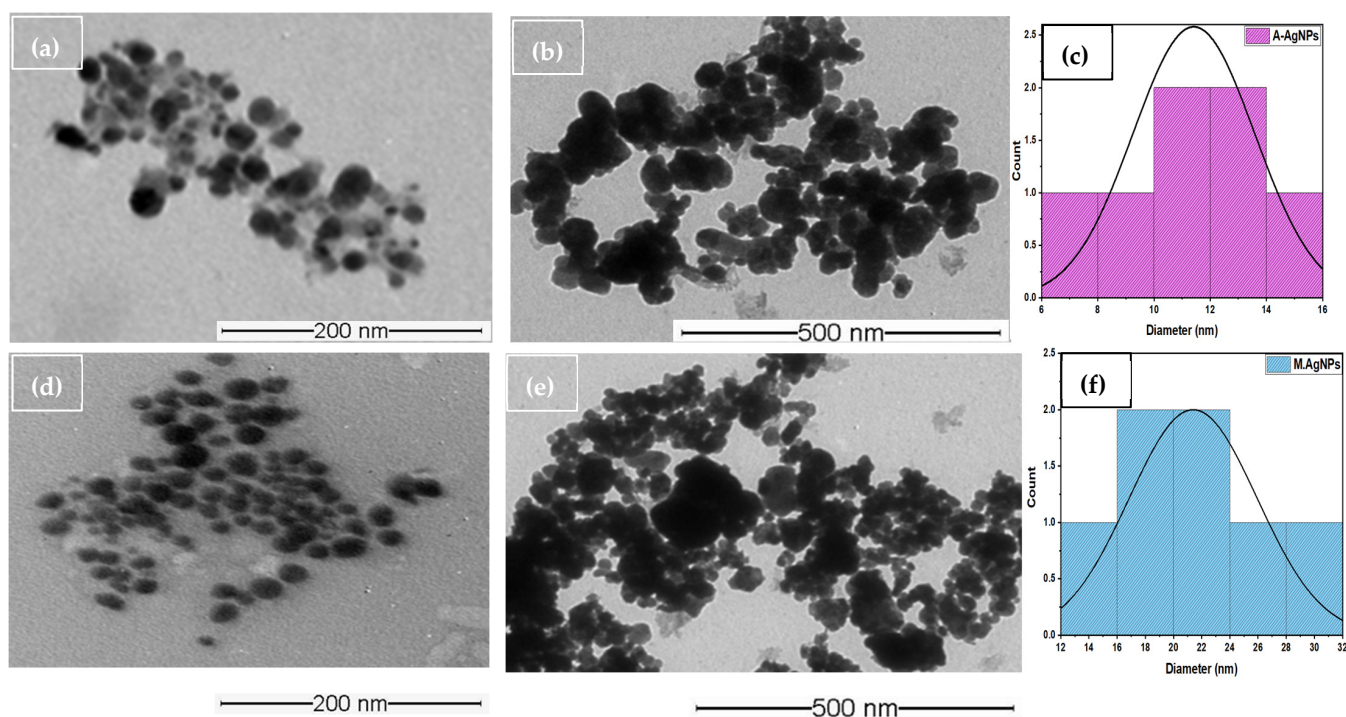


Figure 6. TEM images of spherical monodisperse nanoparticles produced using *A. indica* and *M. indica*. (a–c) *A-AgNPs* under higher magnification and low magnification, as well as a histogram plot representing the average size of NPs; (d–f) High-magnification and low-magnification images, with histogram presenting the size of the *M-AgNPs*.

The aggregation of monodisperse AgNPs was recorded by TEM for the measurements. Previous studies reported by Consolo et al., presented spherical AgNPs with a similar size (5 and 18 nm), synthesized from a strain of *Trichoderma harzianum* fungus [48].

The anti-fungal activity of the AgNPs, presented zones of inhibition of 20 mm and 15 mm against *Pyricularia oryzae* and *A. alternata*, respectively [49].

Khatami et al., also described similar spherical AgNPs with an average size of 1–35 nm synthesized using *Descurainia sophia*, showing good anti-fungal activity. The size of the AgNPs was confirmed by studies suggesting good antimicrobial activity [50].

5.4. SEM (Morphology)

A. indica and *M. indica* tree leaf extracts were used to synthesize the AgNPs, and SEM images were obtained of the leaf extract. The images showed relatively spherical-shaped AgNPs when observed at a magnification of acceleration voltage of 21.84 KX with an angle of 54.00, as shown in Figure 7a at a magnification of 5.00 kV and at low magnification.

For the multilayer deposition of diluted colloidal AgNPs (different NPs) coated on a silicon substrate, the surface morphologies of *A-AgNPs* and *M-AgNPs* synthesized using other plant extracts were spherical at both high and low magnification, with similar results being reported by Torres-Martinez et al., during the synthesis of AgNPs using *Mentha spicata* extract [51]. Comparable results were observed by Agnihotri et al., in immobilized AgNPs on a silica surface, which showed similar uniformly dispersed NPs in a spherical shape. The images of the AgNPs samples indicate their green synthesis, and the particles were spherical in shape, with agglomeration [52]. Similar results were reported by Kiran et al., who synthesized AgNPs using *Eucalyptus tereticornis* leaf extract, and tested them against the MCF-7 cancer cell line [53]. The phytochemicals were present on the surface of the AgNPs, affecting the size of the NPs. The synthesized *A-AgNPs* and *M-AgNPs* were aggregated in the colloidal solution due to the appropriate quality of phytochemicals attached to the AgNPs.

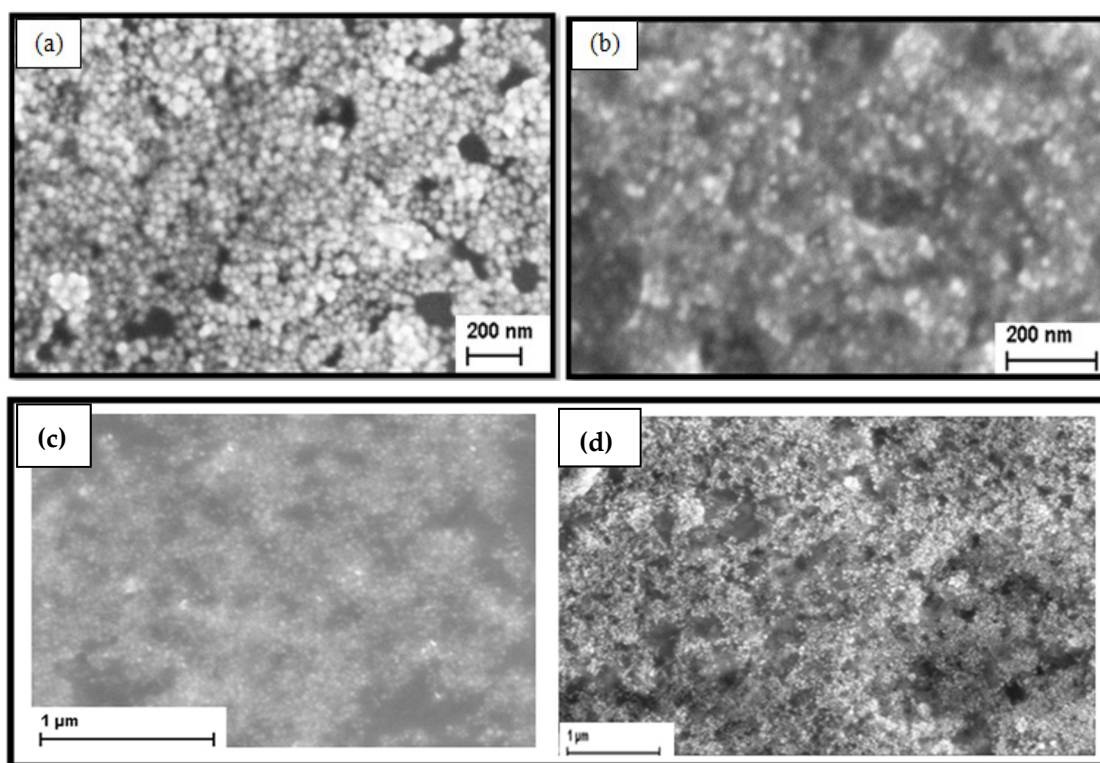


Figure 7. SEM images of AgNPs synthesized using *A. indica* and *M. indica*; (a) *A-AgNPs* and (b) *M-AgNPs* at high magnification; and (c) *A-AgNPs* and (d) *M-AgNPs* at low magnification.

5.5. Particle Size Analysis

The hydrodynamic diameter of the green-synthesized spherical-shaped *A-AgNPs* and *M-AgNPs* was studied using the DLS technique. The surface-active molecules on the surface of the nanoparticles produced stable mono-dispersed colloidal AgNPs. The size of the nanoparticles when measured by DLS (i.e., with a larger size) is dependent on the surrounding metallic core and the thickness of the electrical double layer [54]. The morphology, surface area, composition, particle reactivity, and size distribution of the nanoparticles were observed to be in the range 90–1000 nm. Javed et al., 2020 reported that phytochemicals-capped AgNPs have a large surface area, which plays a vital role in destroying bacteria, fungi, and viruses [55]. As it can be observed from Figure 8a,b the particles were in a monodispersed phase, and the calculated hydrodynamic diameters (average size) of *A-AgNPs* and *M-AgNPs* were 112.4 nm and 125.8 nm. The PDI values of *A-AgNPs* and *M-AgNPs* were calculated on the basis of three measurements, achieving values of 0.216 and 0.2376, respectively. These PDI values further support the inference that the AgNPs are spherical and monodispersed. Mahiuddin et al., studied AgNPs using *Piper Chaba* stem extracts and reported the hydrodynamic size to be 122 nm, with a PDI value of ~0.221, indicating that the NPs were monodisperse [56]. The average size observed through DLS was greater than that observed via TEM due to the capping of phytochemicals on the surface of nanoparticles. The shape and size of nanoparticles is dependent on the temperature, pH, reductant (extract), and precursor concentration [57]. The DLS pattern demonstrates the hydrodynamic diameter of synthesized AgNPs, which is influenced by the phytochemicals adsorbed onto the surface of the NPs. The depth of the electrical double layer, and how it affects the size of the NPs is determined by the presence of AgNPs in colloidal form and on the surface of the NPs. As a result, DLS measurements inflate the size of spherical AgNPs compared to other macroscopic methods [58].

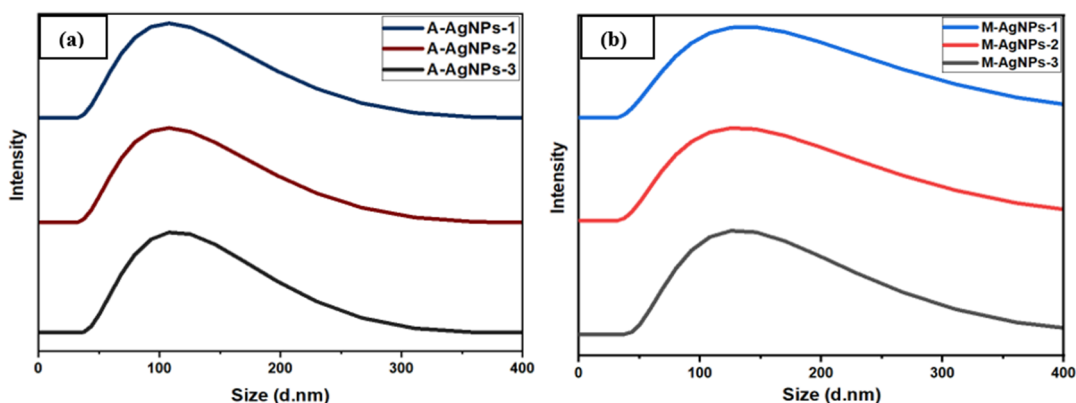


Figure 8. (a,b) Average size of *A-AgNPs* and *M-AgNPs* determined using DLS.

The studies also reported Brownian fluctuations in intensity for smaller particles more than for larger particles [59]. The studies indicate that plant-synthesized NPs aggregate frequently compared to ionic liquids [60]. Similar studies have been published recently by Rana et al., who synthesized AgNPs with a hydrodynamic diameter of 250 nm and a zeta potential value of -13.9 mV [34].

5.6. Stability

The stability of AgNPs was also determined using a Zeta-potential instrument. It is essential to know the parameters of stabilized nanoparticles, as the optimal range for highly stable AgNPs is set to be greater than -30 mV and less than $+30$ mV. The negative zeta potential values of *A-AgNPs* and *M-AgNPs* were found at -19.07 mV and -17.2 mV, indicating the stability of NPs Figure 9a,b. The colloidal form of AgNPs averts aggregation due to repulsion between NPs [61]. The zeta potential also depends on the dispersion of electrolytes and the pH of nanoparticles. The negative charge on the surface of the nanoparticles establishes repulsion between the particles, thus validating their stability. Phanjom et al., synthesized AgNPs and reported similar results for zeta potential, at -14.3 mV [62]. Anandalakshmi et al., reported the zeta potential of AgNPs (*Pedaliium murex* leaf extract) as -7.66 mV, thus demonstrating nanoparticles stability [63]. The negative charge in the functional group of the phytochemicals stabilizes the nanoparticles and prevents them from clustering.

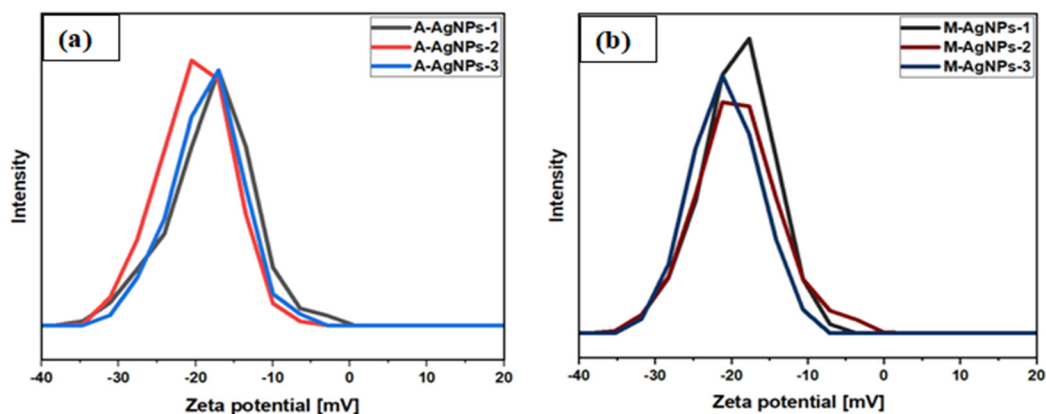


Figure 9. Zeta potential of stable (a) *A-AgNPs* and (b) *M-AgNPs* at ($-$, " 19.07 mV") and ($-$, " 17.2 mV").

5.7. FTIR Spectroscopy Analysis

A phytochemicals analysis was performed to identify the presence of azadirachtin, gallic acid, flavonoids, saponins, alkaloids, and Nimbins, as shown in Figure 10a,b. The peak observed in the FTIR spectrum due to the association between the functional group and absorption bands had the ability to enhance the antimicrobial activities of AgNPs

synthesized using two different plants [64]. The shifting of FTIR bands in the spectrum demonstrates major and minor shifts that could be due to the stabilization, reduction and capping of AgNPs. The FTIR spectrum of *A*-AgNPs showed major absorption peaks at 3680, 3454, 3141, 2968, 2567, 1843, 1256, 1119, 868, 700, and 510 cm^{-1} , which also indicates the presence of phytochemicals (Figure 10a, red). The FTIR spectrum of *A. indica* leaf extract showed major absorption peaks at 3807, 3538, 3251, 2960, 2608, 1945, 1315, 925, 837, and 602 cm^{-1} (Figure 10a, black). Similarly, the FTIR spectrum for *M*-AgNPs showed major absorption peaks for phytochemicals at 3741, 3495, 3405, 3165, 3042, 2873, 2412, 1297, 1132, 809, 559 cm^{-1} (Figure 10b, red). The FTIR spectrum of *M. indica* leaf extract showed major absorption peaks at 3834, 3708, 3575, 3288, 3082, 2648, 2177, 1241, 1142, 984, and 810 cm^{-1} (Figure 10b, black). The peaks observed at 3807, 3741 and 3834 and 3708 cm^{-1} for the strong -OH band stretching vibrations were detected in both samples and plant extract (Figure 10a,b). The peaks observed at 3680, 3538, and 3575 cm^{-1} were assigned to the phenol group present in the phytochemicals. The peaks observed at 3495, 3454, 3405, 3281, 3277, 3288, 3251, 3110, 3141, and 3165 cm^{-1} were assigned to the O-H/N-H/C-H stretching of phenol, amine and amide linkage present in the leaf extract [65].

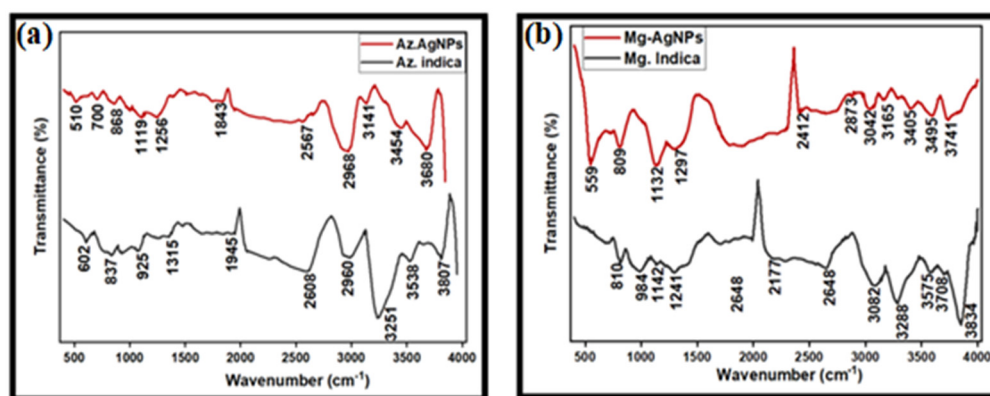


Figure 10. FTIR spectra of biosynthesized (a) *A*-AgNPs and (b) *M*-AgNPs using *A. indica* and *M. indica* extract at 70 °C.

The peaks observed at 3042 and 3082 cm^{-1} were assigned to CH stretching of the aromatic ring. The methyl group, cycloalkane and aliphatic C-H stretching, and carboxylic acid show a peak at 2567, 2608, 2648, 2873 and 2412 cm^{-1} . The carboxylic group in the anhydride functional group exhibits the absorption band at 1843, 1945 cm^{-1} . The peak at 1315, 1256, 1297, and 1241 cm^{-1} were assigned for C-O/C-H bending and alkyl ketone. The alkyl amine group and OH stretching were observed at 1119, 1132, and 1142 cm^{-1} and the band at 1012 cm^{-1} for tertiary alcohol. The ether group (C-O-C) observed the absorption peaks at 925, 984 cm^{-1} . The peaks were observed at 868, 837, 809, 810, and 700 cm^{-1} for C-O and C-S stretching in the aliphatic group. The peaks observed at 602 cm^{-1} are present due to the stretching of the aromatic group, whereas 510 and 559 cm^{-1} show the presence of the OH group of phenolic. The studies show that protein, polysaccharides, amide group, azadirachtin, phenols, alkaloids, carbohydrates, and fatty acids are required in the reduction of silver metal to silver nanoparticles [66]. The peaks from FTIR indicate the presence of phytochemical compounds that conclude the stability, interaction, and synthesis of AgNPs from *A. indica* and *M. indica*. The outcomes of the data do not sync up with the phytochemical testing done on *A. indica* and *M. indica* [65].

5.8. DPPH Scavenging

The aqueous extract of *A. indica* and *M. indica* and their synthesized AgNPs are able to donate electrons or radicals for the study of antioxidant activity by means of DPPH assay as a free radical scavenger.

The antioxidant activity is directly proportional to AgNPs and plant extract concentration. The presence of functional groups in the phytochemicals present in different plants

results in natural antioxidants with high reducing capacity. However, our data indicate that the highest scavenging activity of DPPH was achieved at concentrations of 500 mg/mL, with *A*-AgNPs achieving 85% and *M*-AgNPs 76%, as demonstrated in Figure 11. The results show better antioxidant activity for AgNPs than standard ascorbic acid (72%). Similar results were produced by Menon et al., who determined the antioxidant activity of AgNPs synthesized using the medicinal plant *Acalypha indica* leaf extract [67]. The freshly prepared DPPH exhibited a purple color due to the donation of electrons from the extract and the nanoparticles, stabilizing the DPPH with a maximum absorbance at 517 nm. The mechanism of antioxidant activity of AgNPs was single electron transfer to the DPPH radical. AgNPs have free radical quenching ability due to the antioxidants in the NPs [68]. However, the antioxidant activity determined in the AgNPs was higher than in ascorbic acid. The higher antioxidant activity in the green-synthesized AgNPs decreased the chances of cancer when entering through the food chain, but they demonstrate cell toxicity to some extent [69].

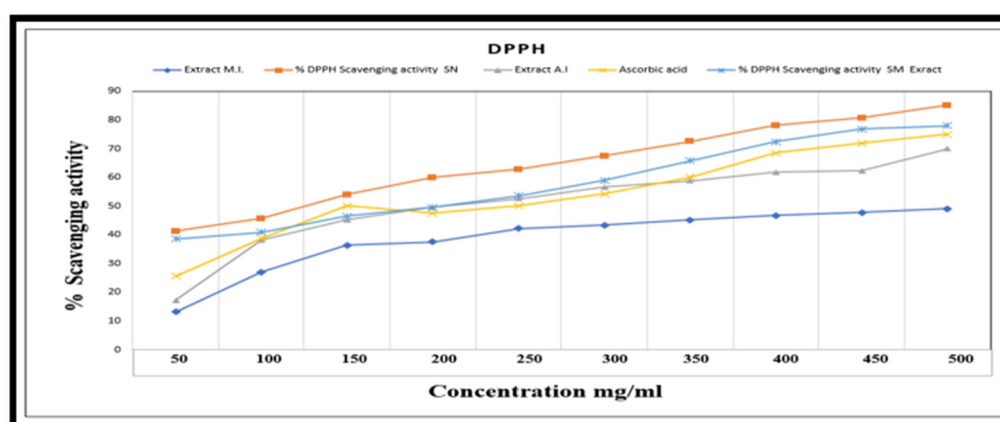


Figure 11. Antioxidant activity of *A*-Ag (*SN*-Silver NPs), *M*-Ag (*SM*-Silver NPs), and their plant extracts.

Antioxidants swiftly scavenge free radicals and gradually block their production, while antimicrobial agents interact with microbes. Both represent different properties; however, under inflammatory conditions, microbial infection highlights that there is a relationship between antioxidant and antimicrobial activities [70]. Compounds with high antioxidant activity may assist specific pathways that produce antimicrobial peptides inside the body. This could result in the inhibition of microbes. According to the study by Farag et al., phenolic compounds have strong antioxidant activities, thus showing the inhibition of microbes by attaching to the active site of an enzyme protein to stop the metabolic process [71]. Farahmandfar et al. reported the antioxidant and antimicrobial activities of *Arum maculatum* extracts, where the highest yield was obtained in ethanol and water (50:50). According to this research, there are phytochemicals like phenols, flavonoids, and tannins that may exchange electrons, and are thus added to foods to prevent peroxidation, rather than preserving them artificially. According to this research, Gram-negative and Gram-positive bacteria are both resistant to the antimicrobial effects of plant extracts with high antioxidant content [72].

5.9. Antimicrobial Activity *A*-AgNPs and *M*-AgNPs

5.9.1. In Vitro Inhibitory Effect of *A*-AgNPs and *M*-AgNPs on *A. alternata* and *A. rolfsii*

The antifungal activity of the green-synthesized AgNPs was investigated on two different plant fungi (*A. alternata* and *A. rolfsii*) pathogens. The diameter of the zone of inhibition with respect to the growth of *A. alternata* fungi was measured with *A*-AgNPs and *M*-AgNPs. The largest zones of inhibition against the *A. alternata* and *A. rolfsii* fungi were observed at a concentration of 10 μ L/mL of *A*-AgNPs and *M*-AgNPs. The smallest zone of inhibition was recorded with a 3 mg/mL concentration of AgNPs. Higher antifungal activity against *A. alternata* and *A. rolfsii* fungi was observed with increasing concentrations

of *A-AgNPs*. The average diameter of the zone of inhibition expanded with increasing concentrations of AgNPs. The *A. alternata* and *A. rolfsii* fungi were tested against *A-AgNPs* and *M-AgNPs* at concentrations of 4 $\mu\text{L}/\text{mL}$, 6 $\mu\text{L}/\text{mL}$, and 10 $\mu\text{L}/\text{mL}$ (denotes as A1, B1, C1 and A2, B2, C2), respectively, for 48 h in (Figure 12a–c). The *A-AgNPs* show larger zones of inhibition for *A. alternata* and *A. rolfsii* fungi than *M-AgNPs*; this could be due to the high degree of synergic antioxidant activity exhibited by *A. indica*. The negative controls (deionized water) did not show any hindrance effect on the growth of fungi.

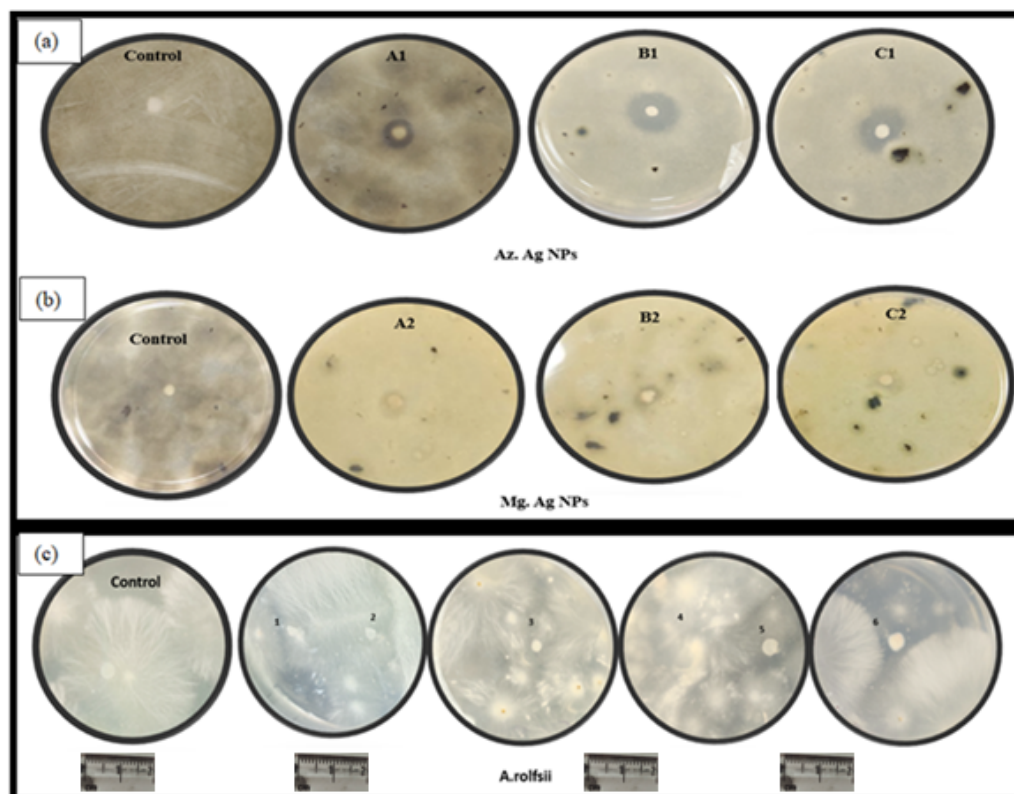


Figure 12. (a) *A-AgNPs* (A1, B1, C1) and (b) *M-AgNPs* (A2, B2, C2) treatment against *A. alternata* and (c) *A. rolfsii* fungi, where *A-AgNPs* (1, 2, 3) and *M-AgNPs* (4, 5, 6) were biosynthesized using *A. indica* and *M. indica*.

5.9.2. Anti-Bacterial Activity

In Vitro Inhibitory Effect of *A-AgNPs* and *M-AgNPs* on the *X. Oryzae* Bacteria

These studies on the growth and inhibition of *X. Oryzae* strain demonstrate that *A-AgNPs* and *M-AgNPs* at different concentrations (6, 8, and 10 $\mu\text{L}/\text{mL}$) inhibit the growth of the bacteria compared with untreated control deionized water. Higher anti-bacterial activity was observed for *A-AgNPs* than *M-AgNPs* against the rice pathogen. The zones of inhibition observed for AgNPs against the bacterium are presented in Figure 13a (1,2,3,4) for *A-AgNPs* and Figure 13b (5,6,7,8) for *M-AgNPs*.

Figure 14 presents the mean of three replicates with the addition of an error bar. The studies were conducted against three different microbes, fungi and bacteria. However, the zone of inhibition was more prone to variance for fungi than for bacteria. A similar study was reported by Rizawan et al., who synthesized AgNPs using *Trigonella foenum-graecum* L. leaf extract, which were spherical in shape, with a size in the range of 9–37 nm and exhibited sharp absorbance peaks at 380 nm. Ampicillin was used as a standard antibiotic for bacterial studies, and Fluconazole and Carbendazim as standard antifungals against fungi tested at the same concentration as the AgNPs against the same microbes [73].

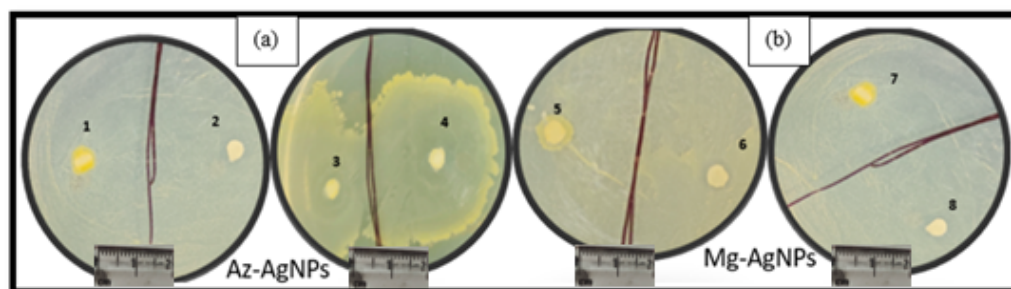


Figure 13. In vitro zone of inhibition effect (mm) of (a) *A-AgNPs* and (b) *M-AgNPs* against *X. Oryzae* bacterial growth on PDA medium after incubation at $27 \pm 1 \text{ }^\circ\text{C}$.

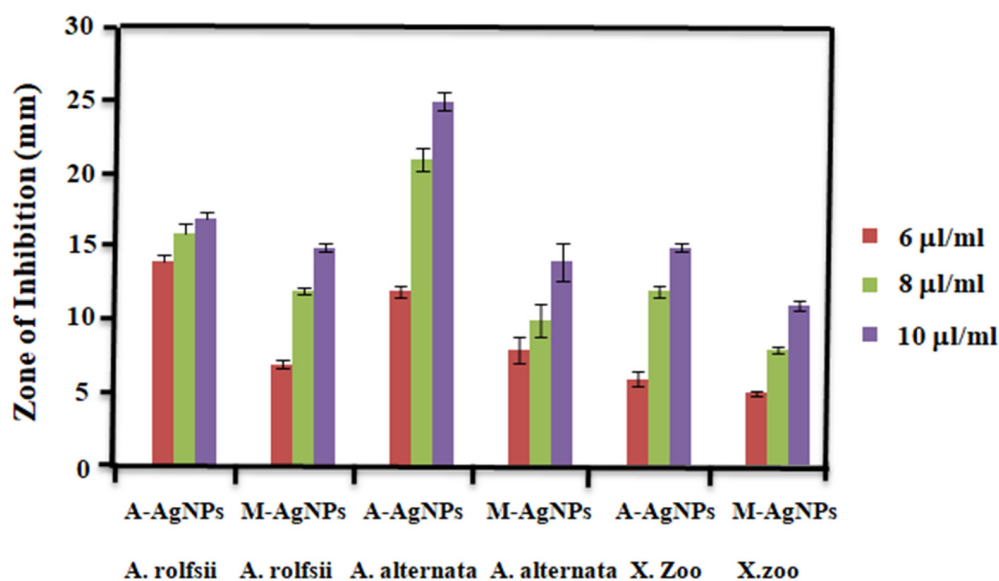


Figure 14. Antimicrobial activity of the AgNPs synthesized using aqueous leaf extract from *A. indica* and *M. indica* tested against *A. rolfsii*, *A. alternata* and *X. Oryzae* microbes. The value represents the mean of three replicates (\pm SD). Analysis of variance showed a significant difference in means ($p < 0.05$).

The AgNPs were tested at three working concentrations, revealing that the lowest MIC (minimum inhibitory concentration) concentration, $6 \mu\text{L}/\text{mL}$, was effective against *A. rolfsii*, *A. alternata* and *X. Oryzae* microbes. Similar results were reported against *P. Aeruginosa* with an MIC value of $0.5 \mu\text{g}/\text{mL}$ [74]. Parvekar et al. studied MIC of AgNPs against *Staphylococcus aureus* bacteria, obtaining an MIC value of $0.625 \text{ mg}/\text{mL}$ [75]. Win et al. synthesized AgNPs using *A. alternata* fungi and evaluated them against *Fusarium moniliforme*, *Fusarium tricinctum*, *Alternaria* sp., and *Fusarium oxysporum*, with the MIC of AgNPs at 25 mL resulting in zones of inhibition of 9–14 mm [31]. Rizwan et al. synthesized AgNPs with a size of 8 nm and 42 nm using *Origanum majorana* extract, and studied their activity against *Alternaria alternata* sp. *lycopersici* and *Pestalotiopsis mangiferae* at concentrations of 4 and $8 \mu\text{L}/\text{mL}$ [76].

6. Discussion

Chemical fertilizers have been used for a long time to manage plant diseases, and as the demand for food increases due to the increasing population, farmers are under increasing pressure to increase crop growth. Excessive use of pesticides in agriculture causes several health issues, including severe allergies. Due to their large surface area and compact size, NPs have been used in agriculture to increase productivity. AgNPs synthesized using plant extract protect and increase the growth of crops. The antimicrobial mechanism of AgNPs is described in Figure 15.

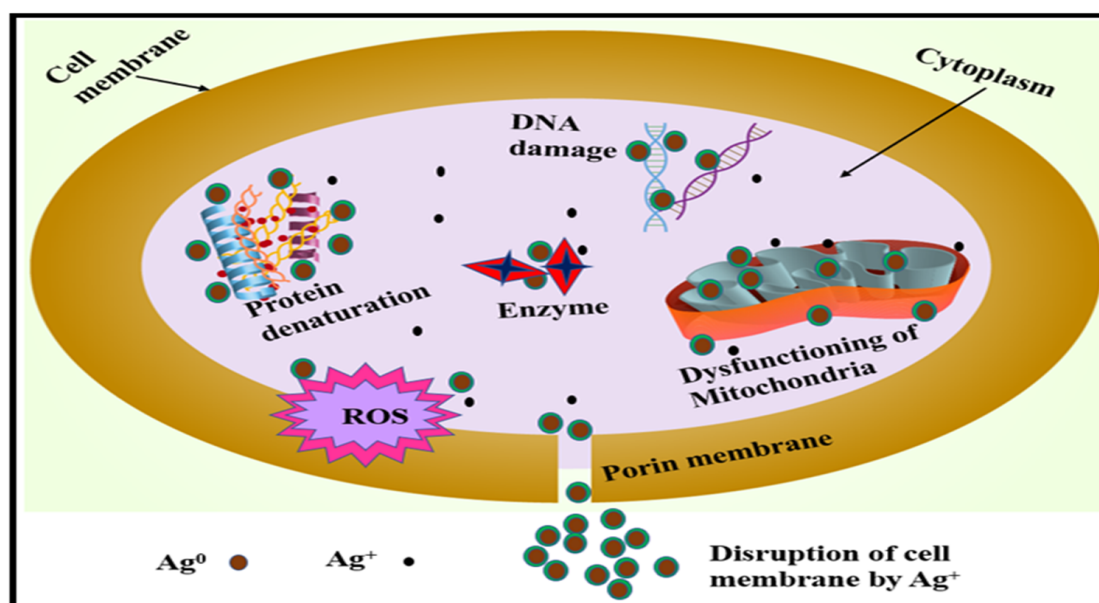


Figure 15. AgNPs mechanism of action for antimicrobial activity. Ag⁺ ions are released from AgNPs during the redox reaction by exchanging electrons and ROS free radicals to react with DNA, protein enzymes, and mitochondria.

The antimicrobial activity of AgNPs studied against plant pathogens disrupts the cell membrane, disrupts the respiration enzyme, and enhances toxicity in microbes by generating ROS, affecting their DNA and RNA and causing cell extinction [77]. The formation of Ag⁺ ions causes the electrostatic interaction of AgNPs through oxidation, which reacts with the negative charge of the cell wall in microbes [78]. Insertion of AgNPs into microbe cells influences the transportation of phosphate ions and thiol groups present in cells for the growth and infection caused in plants and vegetable cells. DNA and RNA structures in cellular carrying cytosine, guanine, pyrimidine, and purine base linked to Ag⁺ ions inhibit the replication of these nucleic acids due to changes in phase from the relaxed state to the condensed state, and also terminate their reproduction [79]. Additionally, free radical species generated by AgNPs when reacting with oxygen during mitochondria metabolism result in methylation breakdown, nitrogenous bases, and carbohydrates [80]. ROS produce hydroxyl, superoxide, hydrogen peroxide, and singlet oxygen, which disorganize the respiratory system of microbes. Sulfur and phosphorous atoms present inside the genome of microbes adhere to the surface of AgNPs, performing electron transfer, thus disturbing respiration and destroying microbes [81]. The mechanism itself explains the importance of plant-derived AgNPs in antimicrobial activities.

Marwah et al., performed similar studies, monitoring the toxicity of chemically synthesized AgNPs at concentrations of 50, 75, and 100 ppm against *Stachybotrys chartarum* fungi, which showed zones of inhibition of 21, 26, and 29 mm, respectively [82]. Previous studies have reported that the AgNPs synthesized using methanolic extract show a similar zone of inhibition when tested against human pathogens, which was recorded at 19.25 mm against *B. cereus* [83]. Recently, Amna et al., carried out similar studies on AgNPs that were 49 nm in size and cubic in shape, which were screened against *Colletotricum falcatum* and *Fusarium moniliforme* fungi, achieving maximum zones of inhibition of 21 mm and 24 mm, respectively [84]. On the basis of the results obtained for both plants for scrutinizing the antimicrobial activity of AgNPs, it was observed that A-AgNPs achieved better results for plant pathogens, fungi, and bacteria. Vanti et al., performed a similar study on the activity of AgNPs synthesized using *Solanum torvum* against *Ralstoniasolana cearum* and *Xanthomonas axonopodis pv. Punicae* bacteria. The highest zones of inhibition were found at 18 mm and 11.4 mm for plant-caused bacteria [85]. Hossain et al. synthesized uniform spherical nanocrystals with a size of 20 to 100 nm for the production of AgNPs using the

bacterium *Pseudomonas rhodesiae*, in order to determine their antibacterial activity against *D. dadantii*, where a maximum zone of inhibition of 22 nm was observed [86]. Ahmed et al., conducted similar studies on the *X. Oryzae* bacteria using AgNPs synthesized from the *Bacillus cereus* strain [87]. Similar work involving *Catharanthus roseus* plant extract was reported by Roy et al., synthesized iron nanoparticles that were resistant to *E. coli* and degraded methyl orange dye by 50% [88]. Salve et al., synthesized AgNPs with an average size of 20 nm using *Madhuca longifolia* leaf extract, which were studied with respect to their anti-inflammatory (protein denaturation) activity against *E. coli* bacteria and their anticancer activity [89]. The AgNPs were found to be spherically shaped, with a size in the range of 18–39 nm, and with respect to their antibacterial activity, showed a zone of inhibition of 25.11 nm. The studies carried out in this paper during the screening of AgNPs with plant pathogens in the absence of any antibiotic demonstrate higher anti-fungal activity than antibacterial activity.

7. Conclusions

This study concludes that green synthesis, which is essential for production of NPs, using *A. indica* and *M. indica* tree leaf extract is environmentally friendly and cost-effective, with natural capping and reducing agents. AgNPs synthesized from plant extract (*A. indica* and *M. indica*) possessed higher antioxidant activity in concentrations ranging from 50 to 500 mg/mL compared with standard ascorbic acid. The green-synthesized AgNPs showed good antimicrobial activity against plant pathogens. However, the *A*-AgNPs and *M*-AgNPs have not been compared together with *A. alternata*, *A. rolfsii* fungi and *X. Oryzae* bacteria. Due to variations in antioxidant and antibacterial levels, these plant extracts demonstrated varying zones of inhibition against microorganisms. *A*-AgNPs proved to possess higher anti-fungal activity than *M*-AgNPs, with a zone of inhibition of 21 and 16 mm, compared to anti-bacterial activity, where the zone of inhibition of 15 mm was highly influenced at a concentration of 6–10 $\mu\text{L}/\text{mL}$. The AgNPs exhibited greater antifungal activity after four days than antibacterial efficacy after two days. The free radical and cation of Ag^+ ions react with sulfur and phosphorous elements. The use of plant extract added many natural benefits to NPs, with less pollution and excellent efficiency in nanotechnology techniques. Therefore, synthesizing AgNPs from leaf extract is a cost-effective, time-saving, and reagent-free way of preparing phytoremediation products to restrict phytopathogen growth. The antimicrobial activity of AgNPs reduces the potency of pathogens, thus preserving the agricultural system.

Author Contributions: A.R.: Conceptualization, Writing—original draft, Methodology, Investigation. A.K.: Resources, Software. A.K.C.: Resources, Software. R.S.: Writing—review & editing. D.K.: Resources, Software. P.V.: Writing—review & editing. S.N.S.: Supervision, Validation, Visualization, Writing—review & editing. All authors have read and agreed to the published version of the manuscript.

Funding: This research was funded by University Grants Commission (UGC) grant number-90802.

Data Availability Statement: Raw data were generated at the National Physical Laboratory and Indian Institute of Agricultural Sciences, Pusa road, New Delhi. All data are presented within the article.

Acknowledgments: The author Archana Rana would like to acknowledge the AcSIR for providing necessary facilities to carry out the experimental work and also thank the University Grants Commission (UGC-90802) for providing Research Fellowship.

Conflicts of Interest: The authors have no competing interest to declare.

Abbreviations

AgNPs	Silver nanoparticles
<i>A. indica</i>	<i>Azadirachta indica</i>
<i>M. indica</i>	<i>Mangifera indica</i>
<i>A. alternata</i>	<i>Alternaria alternata</i>
<i>A. rolfsii</i>	<i>Sclerotium rolfsii</i>
<i>X. oryzae</i>	<i>Xanthomonas oryzae</i>
A-AgNPs	<i>A. indicasilver</i> nanoparticles
M-AgNPs	<i>M. indica</i> silver nanoparticles

References

- Mohanta, Y.K.; Nayak, D.; Biswas, K.; Singdevsachan, S.K.; Abd Allah, E.F.; Hashem, A.; Alqarawi, A.A.; Yadav, D.; Mohanta, T.K. Silver nanoparticles synthesized using wild mushroom show potential antimicrobial activities against food borne pathogens. *Molecules* **2018**, *23*, 655. [[CrossRef](#)] [[PubMed](#)]
- Chen, L.; Huo, Y.; Han, Y.X.; Li, J.F.; Ali, H.; Batjikh, I.; Hurh, J.; Pu, J.Y.; Yang, D.C. Biosynthesis of gold and silver nanoparticles from *Scutellaria baicalensis* roots and in vitro applications. *Appl. Phys. A* **2020**, *126*, 424. [[CrossRef](#)]
- Ahmad, A.; Wei, Y.; Syed, F.; Tahir, K.; Rehman, A.U.; Khan, A.; Ullah, S.; Yuan, Q. The effects of bacteria-nanoparticles interface on the antibacterial activity of green synthesized silver nanoparticles. *Microb. Pathog.* **2017**, *102*, 133–142. [[CrossRef](#)] [[PubMed](#)]
- Kanawaria, S.K.; Sankhla, A.; Jatav, P.K.; Yadav, R.S.; Verma, K.S.; Velraj, P.; Kachhwah, S.; Kothari, S.L. (2018). Rapid biosynthesis and characterization of silver nanoparticles: An assessment of antibacterial and antimycotic activity. *Appl. Phys. A* **2018**, *124*, 320. [[CrossRef](#)]
- Ijaz, M.; Yousaf, M.; El Shafey, A.M. Arrhenius activation energy and Joule heating for Walter-B fluid with Cattaneo–Christov double-diffusion model. *J. Therm. Anal. Calorim.* **2021**, *143*, 3687–3698. [[CrossRef](#)]
- Zhao, L.; Lu, L.; Wang, A.; Zhang, H.; Huang, M.; Wu, H.; Xing, B.; Wang, Z.; Ji, R. Nano-biotechnology in agriculture: Use of nanomaterials to promote plant growth and stress tolerance. *J. Agric. Food Chem.* **2020**, *68*, 1935–1947. [[CrossRef](#)]
- Rai, M.; Ribeiro, C.; Mattaso, L.; Duran, N. *Nanotechnologies in Food and Agriculture*; Springer: Cham, Switzerland, 2016. [[CrossRef](#)]
- Chauhan, N.; Tyagi, A.; Kumar, P.; Malik, A. Antibacterial potential of *Jatropha curcas* synthesized silver nanoparticles against food borne pathogens. *Front. Microbiol.* **2016**, *7*, 1748. [[CrossRef](#)]
- Hubballi, M.; Nakkeeran, S.; Raguchander, T.; Anand, T.; Samiyappan, R. Effect of environmental conditions on growth of *Alternaria alternata* causing leaf blight of noni. *World J. Agric. Sci.* **2010**, *6*, 171–177.
- Gil, M.; Caniga, M.; Eckman, J.; McLeod, R.; Moy, L.; Wilhelm, A.; Woodhouse, J.; Hoover, J.Z.; Cicmil, M. *Alternaria alternata* induced inflammatory lung responses: A novel in vivo PK/PD model. *J. Inflamm.* **2013**, *10*, 10. [[CrossRef](#)]
- Chowdhary, A.; Agarwal, K.; Randhawa, H.S.; Kathuria, S.; Gaur, S.N.; Najafzadeh, M.J.; Roy, P.; Arora, N.; Khanna, G.; Meis, J.F. A rare case of allergic bronchopulmonary mycosis caused by *Alternaria alternata*. *Med. Mycol.* **2012**, *50*, 890–896. [[CrossRef](#)]
- Chen, L.; Wu, Y.D.; Chong, X.Y.; Xin, Q.H.; Wang, D.X.; Bian, K. Seed-borne endophytic *Bacillus velezensis* LHSB1 mediate the biocontrol of peanut stem rot caused by *Sclerotium rolfsii*. *J. Appl. Microbiol.* **2020**, *128*, 803–813. [[CrossRef](#)]
- Angeles-Shim, R.B.; Shim, J.; Vinarao, R.B.; Lapis, R.S.; Singleton, J.J. A novel locus from the wild allotetraploid rice species *Oryza latifolia* Desv. confers bacterial blight (*Xanthomonas oryzae* pv. *oryzae*) resistance in rice (*O. sativa*). *PLoS ONE* **2020**, *15*, e0229155. [[CrossRef](#)]
- Islas, J.F.; Acosta, E.; G-Buentello, Z.; Delgado-Gallegos, J.L.; Moreno-Trevino, M.G.; Escalante, B.; Moreno-Cuevas, J.E. An overview of Neem (*Azadirachta indica*) and its potential impact on health. *J. Funct. Foods* **2020**, *74*, 104171. [[CrossRef](#)]
- Tariq, M.; Mohammad, K.N.; Ahmed, B.; Siddiqui, M.A.; Lee, J. Biological synthesis of silver nanoparticles and prospects in plant disease management. *Molecules* **2022**, *27*, 4754. [[CrossRef](#)]
- Singh, R.; Gupta, A.K.; Patade, V.Y.; Balakrishna, G.; Pandey, H.K.; Singh, A. Synthesis of silver nanoparticles using extract of *Ocimum kilimandscharicum* and its antimicrobial activity against plant pathogens. *SN Appl. Sci.* **2019**, *1*, 1652. [[CrossRef](#)]
- Aritonang, H.F.; Koleangan, H.; Wuntu, A.D. Synthesis of silver nanoparticles using aqueous extract of medicinal plants (Impatiens balsamina and Lantana camara) fresh leaves and analysis of antimicrobial activity. *Int. J. Microbiol.* **2019**, *2019*, 8642303. [[CrossRef](#)]
- Castillo-Henriquez, L.; Alfaro-Aguilar, K.; Ugalde-Álvarez, J.; Vega-Fernández, L.; Montes de Oca-Vásquez, G.; Vega-Baudrit, J.R. Green synthesis of gold and silver nanoparticles from plant extracts and their possible applications as antimicrobial agents in the agricultural area. *Nanomaterials* **2020**, *10*, 1763. [[CrossRef](#)]
- Mohammed, A.E.; Al-Qahtani, A.; Al-Mutairi, A.; Aabed, K.F. Antibacterial and cytotoxic potential of biosynthesized silver nanoparticles by some plant extracts. *Nanomaterials* **2018**, *8*, 382. [[CrossRef](#)]
- Gavamukulya, Y.; Maina, E.N.; Meroka, A.M.; Madivoli, E.S.; El-Shemy, H.A.; Wamunyokoli, F.; Magoma, G. Green Synthesis and Characterization of Highly Stable Silver Nanoparticles from Ethanolic Extracts of Fruits of *Annona muricata*. *J. Inorg. Organomet. Polym. Mater.* **2020**, *30*, 1231–1242. [[CrossRef](#)]
- Ismail, M.; Gul, S.; Khan, M.I.; Khan, M.A.; Asiri, A.M.; Khan, S.B. *Medicago polymorpha*-mediated antibacterial silver nanoparticles in the reduction of methyl orange. *Green Process. Synth.* **2019**, *8*, 118–127. [[CrossRef](#)]

22. Maji, S.; Modak, S. Neem: Treasure of natural phytochemicals. *Chem. Sci. Rev. Lett.* **2021**, *10*, 396–401. [[CrossRef](#)]
23. Kumar, M.; Saurabh, V.; Tomar, M.; Hasan, M.; Changan, S.; Sasi, M.; Maheshwari, C.; Prajapati, U.; Singh, S.; Prajapat, R.K.; et al. Mango (*Mangifera indica* L.) Leaves: Nutritional composition phytochemical profile, and health-promoting bioactivities. *Antioxidants* **2021**, *10*, 299. [[CrossRef](#)] [[PubMed](#)]
24. Pradeep, M.; Kruszka, D.; Kachlicki, P.; Mondal, D.; Franklin, G. Uncovering the Phytochemical Basis and the Mechanism of Plant Extract-Mediated Eco-Friendly Synthesis of Silver Nanoparticles Using Ultra-Performance Liquid Chromatography Coupled with a Photodiode Array and High-Resolution Mass Spectrometry. *ACS Sustain. Chem. Eng.* **2022**, *10*, 562–571. [[CrossRef](#)]
25. Omidi, S.; Sedaghat, S.; Tahvildar, K.; Derakhshi, P.; Motiee, F. Biosynthesis of silver nanoparticles with *adiantum capillus-veneris* L. leaf extract in the batch process and assessment of antibacterial activity. *Green Chem. Lett. Rev.* **2018**, *11*, 544–551. [[CrossRef](#)]
26. Sharma, M.; Yadav, S.; Srivastava, M.; Ganesh, N.; Srivastava, S. Promising anti-inflammatory bio-efficiency of saponin loaded silver nanoparticles prepared from the plant *Madhuca longifolia*. *Asian J. Nanosci. Mater.* **2018**, *1*, 244–261. [[CrossRef](#)]
27. Akintola, A.O.; Kehinde, B.D.; Ayoola, P.B.; Adewoyin, A.G.; Adewoyin, A.G.; Ajayi, J.F.; Ogunsona, S.B. Antioxidant properties of silver nanoparticles biosynthesized from methanolic leaf extract of *Blighia sapida*. *IOP Conf. Ser. Mater. Sci. Eng.* **2020**, *805*, 012004. [[CrossRef](#)]
28. Agrawal, S.; Popli, D.B.; Sircar, K.; Chowdhry, A. A review of the anticancer activity of *Azadirachta indica* (Neem) in oral cancer. *J. Oral Biol. Craniofacial Res.* **2020**, *10*, 206–209. [[CrossRef](#)]
29. Das, R.; Mukherjee, A.; Sinha, I.; Roy, K.; Dutta, B.K. Synthesis of potential bio-adsorbent from Indian Neem leaves (*Azadirachta indica*) and its optimization for malachite green dye removal from industrial wastes using response surface methodology: Kinetics, isotherms and thermodynamic studies. *Appl. Water Sci.* **2020**, *10*, 117. [[CrossRef](#)]
30. Bos, L. Beijerinck's work on tobacco mosaic virus: Historical context and legacy. *Philos. Trans. R. Soc. London Ser. B Biol. Sci.* **1999**, *354*, 675–685. [[CrossRef](#)]
31. Win, T.T.; Khan, S.; Fu, P. Fungus- (*Alternaria* sp.) mediated silver nanoparticles synthesis, characterization, and screening of antifungal activity against some phytopathogens. *J. Nanotechnol.* **2020**, *2020*, 8828878. [[CrossRef](#)]
32. Saion, E.; Gharibshahi, E.; Naghavi, K. Size-Controlled and Optical Properties of Monodispersed Silver Nanoparticles Synthesized by the Radiolytic Reduction Method. *Int. J. Mol. Sci.* **2013**, *14*, 7880–7896. [[CrossRef](#)] [[PubMed](#)]
33. Mohanta, Y.K.; Panda, S.K.; Jayabalan, R.; Sharma, N.; Bastia, A.K.; Mohanta, T.K. Antimicrobial, antioxidant and cytotoxic activity of silver nanoparticles synthesized by leaf extract of *Erythrina suberosa* (Roxb.). *Front. Mol. Biosci.* **2017**, *4*, 14. [[CrossRef](#)] [[PubMed](#)]
34. Rana, A.; Chaudhary, A.K.; Saini, S.; Srivastava, R.; Kumar, M.; Sharma, S.N. Ultrafast Transient Absorption Spectroscopic (UFTAS) and antibacterial Efficacy Studies of Phytofabricated Silver Nanoparticles using *Ocimum Sanctum* Leaf Extract. *Inorg. Chem. Commun.* **2023**, *147*, 110233. [[CrossRef](#)]
35. Nourafkan, E.; Alamdari, A. Modelling of silver nanoparticles synthesis in ternary reverse microemulsion of Cyclohexane/Water/SDS. *Part. Sci. Technol.* **2014**, *32*, 215–223. [[CrossRef](#)]
36. Mangini, V.; Dell'Aglio, M.; Stradis, A.D.; Giacomo, A.D.; Pascale, O.D.; Natile, G.; Arnesano, F. Amyloid Transition of Ubiquitin on Silver Nanoparticles Produced by Pulsed Laser Ablation in Liquid as a Function of Stabilizer and Single-Point Mutations. *Chem. Eur. J.* **2014**, *20*, 10745–10751. [[CrossRef](#)]
37. Khannanov, A.A.; Rossova, A.A.; Ignatyeva, K.A.; Ulakhovich, N.A.; Gerasimov, A.V.; Boldyrev, A.E.; Evtugyn, V.G.; Rogov, A.M.; Cherosov, M.A.; Gilmudtinov, I.F.; et al. Superparamagnetic cobalt nanoparticles in hyperbranched polyester polyol matrix with anti-protease activity. *J. Magn. Magn. Mater.* **2021**, *547*, 168808. [[CrossRef](#)]
38. Meena, R.K.; Meena, R.; Arya, D.K.; Jadoun, S.; Hada, R.; Kumari, R. Synthesis of silver nanoparticles by *Phyllanthus emblica* plant extract and their antibacterial activity. *Mater. Sci. Res. India* **2020**, *17*, 136–145. [[CrossRef](#)]
39. Heydari, R.; Rashidipour, M. Green synthesis of silver nanoparticles using extract of oak fruit hull (Jaft): Synthesis and in vitro cytotoxic effect on MCF-7 cells. *Int. J. Breast Cancer* **2015**, *2015*, 846743. [[CrossRef](#)]
40. Namburi, K.R.; Kora, A.J.; Chetukuri, A.; Kota, V.S.M.K. Biogenic silver nanoparticles as an antibacterial agent against bacterial leaf blight causing rice phytopathogens *Xanthomonas oryzae* pv. *oryzae*. *Bioprocess Biosyst. Eng.* **2021**, *44*, 1975–1988. [[CrossRef](#)]
41. Pawar, O.; Deshpande, N.; Dagade, S.; Waghmode, S.; Nigam Joshi, P. Green synthesis of silver nanoparticles from purple acid phosphatase apoenzyme isolated from a new source *Limonia acidissima*. *J. Exp. Nanosci.* **2015**, *11*, 28–37. [[CrossRef](#)]
42. Manikandan, V.; Velmurugan, P.; Park, J.-H.; Chang, W.-S.; Park, Y.-J.; Jayanthi, P.; Cho, M.; Oh, B.-T. Green synthesis of silver oxide nanoparticles and its antibacterial activity against dental pathogens. *3Biotech* **2017**, *7*, 72. [[CrossRef](#)]
43. Archana; Sharma, S.N.; Srivastava, R. Silver oxide nanoparticles synthesized by green method from *Artocarpus Hetrophyllus* for antibacterial and antimicrobial applications. *Mater. Today Proc.* **2020**, *28*, 332–336. [[CrossRef](#)]
44. Singh, V.; Shrivastava, A.; Wahi, N. Biosynthesis of silver nanoparticles by plants crude extracts and their characterization using UV, XRD, TEM and EDX. *Afr. J. Biotechnol.* **2015**, *14*, 2554–2567. [[CrossRef](#)]
45. Rodenbough, P.P. *Crystallite Size Dependency of the Pressure and Temperature Response in Nanoparticles of Ceria and Other Oxides*; Columbia University: New York, NY, USA, 2016.
46. Sur, U.K.; Ankamwar, B.; Karmakar, S.; Halder, A.; Das, P. Green synthesis of Silver nanoparticles using the plant extract of *Shikakai* and *Reetha*. *Mater. Today Proc.* **2018**, *5*, 2321–2329. [[CrossRef](#)]
47. Sajanlal, P.R.; Sreepasad, T.S.; Samal, A.K.; Pradeep, T. SAnisotropic nanomaterials: Structure, growth, assembly, and functions. *Nano Rev.* **2011**, *2*, 5883. [[CrossRef](#)]

48. Abdallah, Y.; Liu, M.; Ogunyemi, S.O.; Ahmed, T.; Fouad, H.; Abdelazez Yan, C.; Yang, Y.; Chen, J.; Li, B. Bioinspired green synthesis of chitosan and zinc oxide nanoparticles with strong antibacterial activity against rice pathogen *Xanthomonas oryzae*. *Molecules* **2020**, *25*, 4795. [[CrossRef](#)]
49. Consolo, V.F.; Torres-Nicolini, A.; Alvarez, V.A. Mycosynthetized Ag, CuO and ZnO nanoparticles from a promising *Trichoderma harzianum* strain and their antifungal potential against important phytopathogens. *Sci. Rep.* **2020**, *10*, 1–9. [[CrossRef](#)]
50. Khatami, M.; Mehnipor, R.; Poor, M.H.S. Facile biosynthesis of silver nanoparticles using *Descurainiasophia* and evaluation of their antibacterial and antifungal properties. *J. Clust. Sci.* **2016**, *27*, 1601–1612. [[CrossRef](#)]
51. Torres-Martínez, Y.; Arredondo-Espinoza, E.; Puente, C.; González-Santiago, O.; Pineda-Aguilar, N.; Balderas-Rentería, I.; López, I.; Ramírez-Cabrera, M.A. Synthesis of silver nanoparticles using a *Mentha spicata* extract and evaluation of its anticancer and cytotoxic activity. *PeerJ* **2019**, *7*, e8142. [[CrossRef](#)]
52. Agnihotri, S.; Mukherji, S.; Mukherji, S. Immobilized silver nanoparticles enhance contact killing and show the highest efficacy: Elucidation of the mechanism of bactericidal action of silver. *Nanoscale* **2013**, *5*, 7328–7340. [[CrossRef](#)]
53. Kiran, M.S.; Betageri, V.S.; Ranjuth kumar, C.R.; Vinay, S.P.; Latha, M.S. In-Vitro Antibacterial, Antioxidant and Cytotoxic Potential of Silver Nanoparticles Synthesized Using Novel *Eucalyptus tereticornis* Leaves Extract. *J. Inorg. Organomet. Polym. Mater.* **2020**, *30*, 2916–2925. [[CrossRef](#)]
54. Singh, K.; Panghal, M.; Kadyan, S.; Chaudhary, U.; Yadav, J.P. Green silver nanoparticles of *Phyllanthusamarus*: As an antibacterial agent against multi drug resistant clinical isolates of *Pseudomonas aeruginosa*. *J. Nanobiotechnol.* **2014**, *12*, 40. [[CrossRef](#)]
55. Javed, B.; Akhtar, N. Optimization, characterization and antimicrobial activity of silver nanoparticles against plant bacterial pathogens phyto-synthesized by *Mentha longifolia*. *Mater. Res. Express* **2020**, *7*, 085406. [[CrossRef](#)]
56. Mahiuddin, M.; Saha, P.; Ochiai, B. Green synthesis and catalytic activity of silver nanoparticles based on *Piper chaba* stem extracts. *Nanomaterials* **2020**, *10*, 1777. [[CrossRef](#)]
57. Gurunathan, S.; Kalishwaralal, K.; Vaidyanathan, R.; Pandian, S.R.; Muniyandi, J.; Hariharan, N.; Eom, S.H. Biosynthesis, purification and characterization of silver nanoparticles using *Escherichia coli*. *Colloids Surf. B Biointerfaces* **2009**, *74*, 328–335. [[CrossRef](#)]
58. Tomaszewska, E.; Soliwoda, K.; Kadziola, K.; Tkacz-Szczesna, B.; Celichowski, G.; Cichomski, M.; Szmaja, W.; Grobelny, J. Detection limits of DLS and UV-Vis spectroscopy in characterization of polydisperse nanoparticles colloids. *J. Nanomater.* **2013**, *2013*, 313081. [[CrossRef](#)]
59. Karmakar, S. Particle Size Distribution and Zeta Potential Based on Dynamic Light Scattering: Techniques to Characterise Stability and Surface distribution of Charged Colloids. In *Recent Trends in Materials Physics and Chemistry*; Studium Press (India) Pvt Ltd.: New Delhi, India, 2019; pp. 117–159.
60. Meva, F.E.; Ntumba, A.A.; Kedi, P.B.E. Silver and palladium nanoparticles produced using a plant extract as reducing agent, stabilized with an ionic liquid: Sizing by X-ray powder diffraction and dynamic light scattering. *J. Mater. Res. Technol.* **2019**, *8*, 1991–2000. [[CrossRef](#)]
61. Nagar, N.; Devra, V. A kinetic study on the degradation and biodegradability of silver nanoparticles catalyzed Methyl Orange and textile effluents. *Heliyon* **2019**, *5*, e01356. [[CrossRef](#)]
62. Phanjom, P.; Ahmed, G. Biosynthesized of Silver Nanoparticles by *Aspergillus oryzae* (MTCC No. 1846) and Its Characterizations. *Nanosci. Nanotechnol.* **2015**, *5*, 14–21. [[CrossRef](#)]
63. Anandalakshmi, K.; Venugobal, J.; Ramasamy, V.J.A.N. Characterization of silver nanoparticles by green synthesis method using *Petalium murex* leaf extract and their antibacterial activity. *Appl. Nanosci.* **2016**, *6*, 399–408. [[CrossRef](#)]
64. Pirtarighat, S.; Ghannadnia, M.; Baghshahi, S. Green synthesis of silver nanoparticles using the plant extract of *Salvia spinosa* grown in vitro and their antibacterial activity assessment. *J. Nanostruct. Chem.* **2019**, *9*, 1–9. [[CrossRef](#)]
65. Hemlata; Meena, P.R.; Singh, A.P.; Tejavath, K.K. Biosynthesis of silver nanoparticles using *Cucumis prophetarum* aqueous leaf extract and their antibacterial and antiproliferative activity against cancer cell lines. *ACS Omega* **2020**, *5*, 5520–5528. [[CrossRef](#)] [[PubMed](#)]
66. Tomah, A.A.; Alamer, I.S.A.; Li, B.; Zhang, J.Z. Mycosynthesis of Silver Nanoparticles Using Screened *Trichoderma* Isolates and Their Antifungal Activity against *Sclerotinia sclerotiorum*. *Nanomaterials* **2020**, *10*, 1955. [[CrossRef](#)]
67. Menon, S.; Agarwal, H.; Kumar, S.R.; Kumar, S.V. Green synthesis of silver nanoparticles using medicinal plant *Acalypha indica* leaf extracts and its application as an antioxidant and antimicrobial agent against foodborne pathogens. *Int. J. Appl. Pharm.* **2017**, *9*, 42–50. [[CrossRef](#)]
68. Bedlovičová, Z.; Strapáč, I.; Baláž, M.; Salayová, A. A brief overview on antioxidant activity determination of silver nanoparticles. *Molecules* **2020**, *25*, 3191. [[CrossRef](#)]
69. Shanmugasundaram, T.; Radhakrishnan, M.; Gopikrishnan, V.; Pazhanimurugan, R.; Balagurunathan, R. A study of the bactericidal, anti-biofouling, cytotoxic and antioxidant properties of actinobacterially synthesised silver nanoparticles. *Colloids Surf. B Biointerfaces* **2013**, *111*, 680–687. [[CrossRef](#)]
70. Kurutas, E.B. The importance of antioxidants which play the role in cellular response against oxidative/nitrosative stress: Current state. *Nutr. J.* **2016**, *15*, 71. [[CrossRef](#)]
71. Farag, R.S.; Badei, A.Z.M.A.; Hewedi, F.M.; El-Baroty, G.S.A. Antioxidant activity of some spice essential oils on linoleic acid oxidation in aqueous media. *J. Am. Oil Chem. Soc.* **1989**, *66*, 792–799. [[CrossRef](#)]

72. Farahmandfar, R.; Kenari, R.E.; Asnaashari, M. Bioactive compounds, antioxidant and antimicrobial activities of *Arum maculatum* leaves extracts as affected by various solvents and extraction methods. *Food Sci. Nutr.* **2019**, *7*, 465–475. [[CrossRef](#)]
73. Rizwana, H.; Alwhibi, M.S.; Aldarson, H.A. Green synthesis, characterization, and antimicrobial activity of silver nanoparticles prepared using *Trigonella foenum-graecum* L. leaves grown in Saudi Arabia. *Green Process. Synth.* **2021**, *10*, 421–429. [[CrossRef](#)]
74. Gandham, R.G.; Rohan, B. Green synthesis and antibacterial activity of silver nanoparticles from the aqueous extracts of *Cassia alata*. *Lett. Appl. NanoBioSci.* **2020**, *9*, 1037–1041. [[CrossRef](#)]
75. Parvekar, P.; Palaskar, J.; Metgud, S.; Maria, R.; Dutta, S. The minimum inhibitory concentration (MIC) and minimum bactericidal concentration (MBC) of silver nanoparticles against *Staphylococcus aureus*. *Biomater. Investig. Dent.* **2020**, *7*, 105–109. [[CrossRef](#)] [[PubMed](#)]
76. Rizwana, H.; Alzahrani, T.; Alwhibi, M.S.; Aljowaie, R.M.; Aldehaish, H.A.; Alsaggabi, N.S.; Ramadan, R. Phytofabrication of Silver Nanoparticles and Their Potent Antifungal Activity against Phytopathogenic Fungi. *Processes* **2022**, *10*, 2558. [[CrossRef](#)]
77. Dakal, T.C.; Kumar, A.; Majumdar, R.S.; Yadav, V. Mechanistic basis of antimicrobial actions of silver nanoparticles. *Front. Microbiol.* **2016**, *7*, 1831. [[CrossRef](#)]
78. Choi, O.; Yu, C.P.; Fernández, G.E.; Hu, Z. Esteban Fernández, and Zhiqiang Hu Interactions of nanosilver with *Escherichia coli* cells in planktonic and biofilm cultures. *Water Res.* **2010**, *44*, 6095–6103. [[CrossRef](#)]
79. Arya, G.; Sharma, N.; Mankamna, R.; Nimesh, S. Antimicrobial silver nanoparticles: Future of nanomaterials. In *Microbial Nanobionics*; Springer: Cham, Switzerland; Berlin/Heidelberg, Germany, 2019; pp. 89–119. [[CrossRef](#)]
80. Singh, R.; Cheng, S.; Singh, S. Oxidative stress-mediated genotoxic effect of zinc oxide nanoparticles on *Deinococcus radiodurans*. *3Biotech* **2020**, *10*, 1–13. [[CrossRef](#)]
81. Hamouda, R.A.; Hussein, M.H.; Abo-Elmagd, R.A.; Bawazir, S.S. Bawazir Synthesis and biological characterization of silver nanoparticles derived from the cyanobacterium *Oscillatoria limnetica*. *Sci. Rep.* **2019**, *9*, 1–17. [[CrossRef](#)]
82. Marwah, M.B. Evaluation of silver nanoparticles toxicity against toxic black mold *Stachybotrys chartarum*. *J. Plant Pathol. Microbiol.* **2017**, *8*, 1000408. [[CrossRef](#)]
83. Devi, M.; Devi, S.; Sharma, V.; Rana, N.; Bhatia, R.K.; Bhatt, A.K. Green synthesis of silver nanoparticles using methanolic fruit extract of *Aegle marmelos* and their antimicrobial potential against human bacterial pathogens. *J. Tradit. Complement. Med.* **2019**, *10*, 158–165. [[CrossRef](#)]
84. Amna; Mahmood, T.; Khan, U.N.; Amin, B.; Javed, M.T.; Mehmood, S.; Farooq, M.A.; Sultan, T.; Munis, M.F.H.; Chaudhary, H.J. Characterization of bio-fabricated silver nanoparticles for distinct anti-fungal activity against sugarcane phytopathogens. *Microsc. Res. Tech.* **2021**, *84*, 1522–1530. [[CrossRef](#)]
85. Vanti, G.L.; Kurjogi, M.; Basavesha, K.N.; Teradal, N.L.; Masaphy, S.; Nargund, V.B. Synthesis and antibacterial activity of solanum torvum mediated silver nanoparticle against *Xanthomonas axonopodis* sp. *punicae* and *Ralstonia solanacearum*. *J. Biotechnol.* **2020**, *309*, 20–28. [[CrossRef](#)] [[PubMed](#)]
86. Hossain, A.; Hong, X.; Ibrahim, E.; Li, B.; Sun, G.; Meng, Y.; Wang, Y.; An, Q. Green synthesis of silver nanoparticles with culture supernatant of a bacterium *Pseudomonas rhodesiae* and their antibacterial activity against soft rot pathogen *Dickeya dadantii*. *Molecules* **2019**, *24*, 2303. [[CrossRef](#)]
87. Ahmed, T.; Shahid, M.; Noman, M.; Niazi, M.B.K.; Mahmood, F.; Manzoor, I.; Zhang, Y.; Li, B.; Yang, Y.; Yan, C.; et al. Silver nanoparticles synthesized by using *Bacillus cereus* SZT1 ameliorated the damage of bacterial leaf blight pathogen in rice. *Pathogens* **2020**, *9*, 160. [[CrossRef](#)]
88. Roy, A.; Singh, V.; Sharma, S.; Ali, D.; Azad, A.K.; Kumar, G.; Emran, T.B. Antibacterial and Dye Degradation Activity of Green Synthesized Iron Nanoparticles. *J. Nanomater.* **2022**, *2022*, 3636481. [[CrossRef](#)]
89. Salve, P.; Vinchurkar, A.; Raut, R.; Chondekar, R.; Lakkakula, J.; Roy, A.; Hossain, M.J.; Alghamdi, S.; Almeahmadi, M.; Abdulaziz, O.; et al. An Evaluation of Antimicrobial, Anticancer, Anti-Inflammatory and Antioxidant Activities of Silver Nanoparticles Synthesized from Leaf Extract of *Madhuca longifolia* Utilizing Quantitative and Qualitative Methods. *Molecules* **2022**, *27*, 6404. [[CrossRef](#)] [[PubMed](#)]

Disclaimer/Publisher's Note: The statements, opinions and data contained in all publications are solely those of the individual author(s) and contributor(s) and not of MDPI and/or the editor(s). MDPI and/or the editor(s) disclaim responsibility for any injury to people or property resulting from any ideas, methods, instructions or products referred to in the content.